Check for updates

JGR Oceans

RESEARCH ARTICLE
10.1029/2020JC016738

Estuarine Circulation, Mixing, and Residence Times in the Salish Sea

P. MacCready[1], R. M. McCabe[2,3], S. A. Siedlecki[4], M. Lorenz[5], S. N. Giddings[6], J. Bos[7], S. Albertson[7], N. S. Banas[8], and S. Garnier[8]

[1]University of Washington, School of Oceanography, Seattle, WA, USA, [2]University of Washington, Joint Institute for the Study of the Atmosphere and Ocean, Seattle, WA, USA, [3]University of Washington, Cooperative Institute for Climate, Ocean, and Ecosystem Studies, Seattle, WA, USA, [4]Department of Marine Sciences, University Connecticut, Groton, CT, USA, [5]Leibniz Institute for Baltic Sea Research Warnemünde, Rostock, Germany, [6]University of California, San Diego, La Jolla, CT, USA, [7]Washington State Department of Ecology, Lacey, WA, USA, [8]University of Strathclyde, Glasgow, UK

Abstract A realistic numerical model is used to study the circulation and mixing of the Salish Sea, a large, complex estuarine system on the United States and Canadian west coast. The Salish Sea is biologically productive and supports many important fisheries but is threatened by recurrent hypoxia and ocean acidification, so a clear understanding of its circulation patterns and residence times is of value. The estuarine exchange flow is quantified at 39 sections over 3 years (2017–2019) using the Total Exchange Flow method. Vertical mixing in the 37 segments between sections is quantified as opposing vertical transports: the efflux and reflux. Efflux refers to the rate at which deep, landward-flowing water is mixed up to become part of the shallow, seaward-flowing layer. Similarly, reflux refers to the rate at which upper layer water is mixed down to form part of the landward inflow. These horizontal and vertical transports are used to create a box model to explore residence times in a number of different sub-volumes, seasons, and years. Residence times from the box model are generally found to be longer than those based on simpler calculations of flushing time. The longer residence times are partly due to reflux, and partly due to incomplete tracer homogenization in sub-volumes. The methods presented here are broadly applicable to other estuaries.

Plain Language Summary The Salish Sea is a large estuarine system that includes the cities of Vancouver on the Strait of Georgia and Seattle on Puget Sound. Despite the many rivers flowing into the Salish Sea, the water in the system is mostly ocean water, and there is rapid exchange with the ocean. This exchange is important because it brings in most of the nutrients that feed the ecosystem, and it flushes the system relatively rapidly, leading to generally good water quality. Nonetheless, there are places and times in the Salish Sea that experience problems like hypoxia and fish kills. The goal of this work is to clearly describe the patterns of circulation and mixing throughout the Salish Sea so that we may understand the causes and potential future changes in these water quality problems. We use a realistic computer simulation, tested against many observations, to predict the circulation and mixing patterns. We then use those currents to estimate residence times in different parts of the Salish Sea for different seasons and years. The most important result is that we find that the mixing of surface water with deep water can distribute water properties throughout the Salish Sea, increasing the residence time.

Key Points:

- The estuarine circulation throughout the Salish Sea is estimated over 3 years from a realistic numerical model, focusing on the exchange flow
- The vertical mixing, or "reflux" is stronger at sills, but is also large when integrated over the basins between sills
- Residence time is calculated in three ways, quantifying the extent to which it is increased (often more than doubled) by reflux and incomplete homogenization within a volume

Supporting Information:

- Supporting Information S1

Correspondence to:
P. MacCready,
pmacc@uw.edu

Citation:
MacCready, P., McCabe, R. M., Siedlecki, S. A., Lorenz, M., Giddings, S. N., Bos, J., et al. (2021). Estuarine circulation, mixing, and residence times in the Salish Sea. *Journal of Geophysical Research: Oceans*, *126*, e2020JC016738. https://doi.org/10.1029/2020JC016738

Received 21 AUG 2020
Accepted 14 DEC 2020

© 2020. The Authors.
This is an open access article under the terms of the Creative Commons Attribution-NonCommercial-NoDerivs License, which permits use and distribution in any medium, provided the original work is properly cited, the use is non-commercial and no modifications or adaptations are made.

1. Introduction

The exchange flow is widely recognized as a defining property of tidally averaged estuarine circulation. The persistent inflow of deep, salty water and outflow of shallow, somewhat fresher water is often many times greater in volume flux than all the rivers entering a system. As a result, the exchange flow controls residence times and biogeochemical gradients. Physically this circulation is a result of the density contrast between ocean and river water, combined with mixing and advection from tidal currents (Geyer & MacCready, 2014; MacCready & Geyer, 2010). The theory of estuarine exchange flow was developed and tested for shallow, straight coastal plain estuaries such as the Hudson (Hansen & Rattray, 1965; Ralston et al., 2008) but is less well-developed for more complex systems. In this paper we focus on the circulation of one of these complex systems—the Salish Sea, a large, interconnected system of very deep basins and shallow straits forced by

strong tides and many rivers. Despite the extreme bathymetric irregularity of the Salish Sea, it develops a vigorous exchange flow (Bretschneider et al., 1985; Geyer & Cannon, 1982; D. A. Sutherland et al., 2011; Thomson et al., 2007). The deep inflow and shallow outflow through the mouth of the system average around 140,000 $m^3 s^{-1}$, about 70% of the flow of the Amazon River. This is one of the largest exchange flows on the planet, although it is only about 1/7th the magnitude of the inverse estuarine circulation of the Mediterranean Sea (Pinardi et al., 2019).

A key insight of early researchers was that the Salish Sea may be thought of as a system of large, relatively quiescent basins, joined by straits with strong tidal currents and mixing (Ebbesmeyer & Barnes, 1980). The mixing at straits causes "reflux" in which a significant amount, perhaps up to half (Ebbesmeyer et al., 1988) of the outflowing branch of the exchange flow is mixed down and becomes part of the inflowing branch of the exchange flow. The implications for residence time were recognized immediately: refluxing could mean that it takes much longer for the system to flush out conservative tracers. The mathematical framework for reflux was developed rigorously by Cokelet and Stewart (1985) calling it "efflux/reflux" (efflux is the water mixed up which then heads seaward; reflux is the water mixed down which then heads landward). In the present work we use 3 years of a realistic numerical simulation and new analytical tools to calculate the size and consequences of exchange and reflux in the Salish Sea.

A history of circulation studies in the region is given in Section 2. The model setup and evaluation against data are presented in Section 3, with more detail given in the Supplementary text. The analysis of model fields to calculate the exchange flow and efflux/reflux throughout the system is given in Section 4. A box model is constructed using these transports. Box model results focusing on the residence time are given in Section 5. Further discussion is provided in Section 6.

We find that the exchange flow varies smoothly along the system, increasing nearly linearly from the landward bays to the seaward end at the Strait of Juan de Fuca (Figure 1), consistent with findings in D. A. Sutherland et al. (2011). This finding is not consistent with the exchange flow being interrupted at the sills as hypothesized in Ebbesmeyer and Barnes (1980). This smooth variation we find is often seen in coastal plain estuaries, but is perhaps not expected in a place like the Salish Sea where mixing is tightly concentrated at a few energetic sills (Ebbesmeyer et al., 1988; Gregg & Pratt, 2010; Seim & Gregg, 1994). Use of the Total Exchange Flow (TEF) method (MacCready, 2011) is required for correct estimation of the exchange flow in places where the salt flux is significantly influenced by tidal correlation of salinity and transport. We also find that the vertical efflux/reflux transports, while strongest at sills, are also important throughout the basins when considered as an area integral. The box model is used to calculate the movement of passive tracers in the Salish Sea in different years and seasons. From it we find that residence times which account for reflux, and for incomplete homogenization within basins, may be two or more times longer than standard flushing times.

2. A Brief History of Studies of Salish Sea Circulation

The pattern and variability of circulation, mixing, and water properties in the Salish Sea has been the subject of many studies in the past 7 decades. The overall conclusion is that the system functions like an estuary, with strong, localized mixing and a very large exchange flow despite the fjord-like, glacier-carved basins. Early data on water properties in Puget Sound was collected in 1952–1966 and presented in hand-contoured plots in Collias et al. (1974). Similarly, Crean and Ages (1971) present observations from 12 cruises in 1968 in the Straits of Georgia and Juan de Fuca (see Figure 1 for place names). Early studies of Juan de Fuca prompted its inclusion as an extreme end member in the famous Hansen and Rattray (1965) paper on the physics of the estuarine exchange flow.

Spurred by concerns over the fate of contaminants in the system and the causes of hypoxia, observational studies accelerated greatly in the 1970s. Early Canadian research is reviewed in LeBlond (1983), highlighting important current meter observations of the average exchange flow in Juan de Fuca and Johnstone Strait (the channel at the northern end of Strait of Georgia that connects to the Pacific). On the U.S. side of the international border the National Oceanic and Atmospheric Administration (NOAA) initiated the Marine Ecosystems Analysis Puget Sound Program, with results reviewed in Ebbesmeyer et al. (1988) and many NOAA reports. Simultaneously, large advances were made in understanding the complex pattern

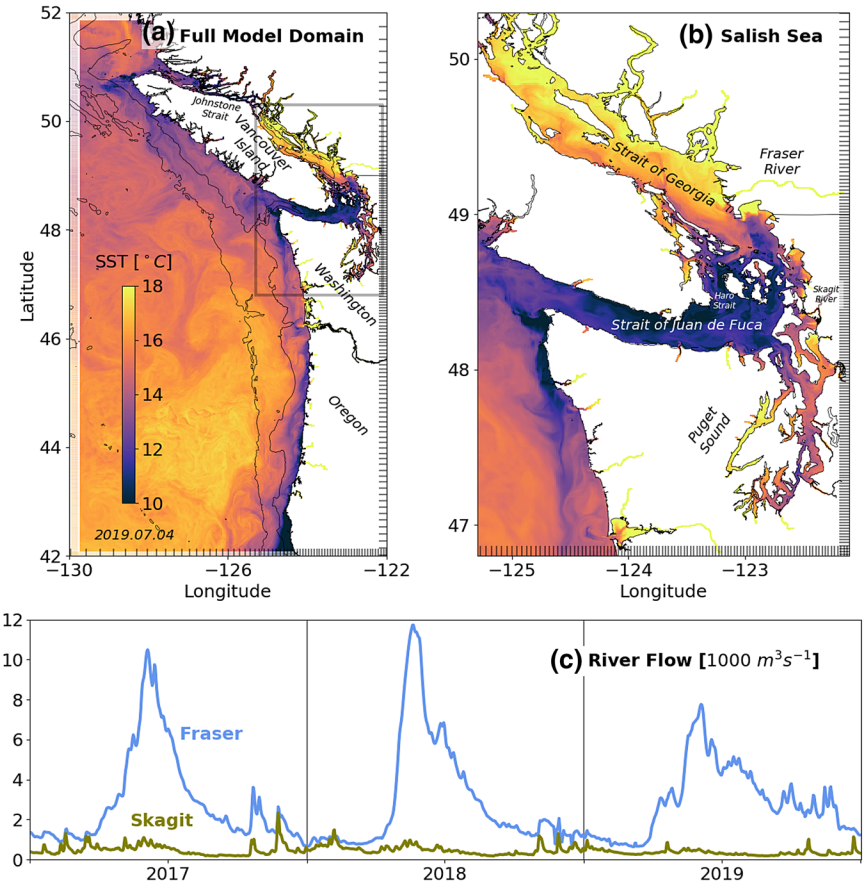

Figure 1. LiveOcean model domain (a) colored by sea surface temperature for July 4, 2019. Grid spacing is indicated with tick marks (only every 10th grid point is drawn). Region of nudging to climatology at open boundaries is indicated by transparency. Bathymetry contours for 200 m and 2,000 m are plotted as black lines. Close up of the model (b) for the Salish Sea with ticks for every fourth grid point. 3-year time series (c) of flow in the Fraser and Skagit Rivers, year is labeled at the middle of the year.

of tides (Lavelle et al., 1988; Mofjeld & Larsen, 1984) that are the dominant factor governing currents and mixing in the Salish Sea. While Puget Sound has been the subject of a great deal of study, it only comprises about 8% of the nearly 2,000 km^3 volume of the Salish Sea.

In the 4 decades since 1980, there have been many observational studies of the Salish Sea ecosystem and circulation. Notable additions to our knowledge have come from the accumulation of long time series from sustained observational programs such as the extensive seasonal surveys conducted by the Canadian Institute of Ocean Sciences (Masson & Peña, 2009), and the Washington (WA) State Department of Ecology monthly (conductivity, temperature, depth) CTD stations initiated around 1990. Long-term change and interannual variability are summarized in Riche et al. (2014) where the gradual warming of the system, and other changes, are made apparent.

Evolving with, and somewhat lagging behind the observational advances, modeling has emerged as a useful scientific tool for Salish Sea studies. The fact that accurate three-dimensional models of the system only arrived in the last decade is due to the extreme bathymetric complexity of the Salish Sea. This complexity prompted the early creation of simpler models that could be used to predict high-value quantities such as residence time. These typically divide the region into a number of segments horizontally and two layers vertically. Cokelet et al. (1991) developed such a model for Puget Sound, exploiting the Knudsen (1900) relations to diagnose the exchange flow from known river flow and salinity distributions; see Burchard et al. (2018) for a translation of Knudsen's paper. A similar approach, allowing for time-dependence, is

presented in Hagy et al. (2000) for a tributary of the Chesapeake. Li et al. (1999) used a more dynamical approach in a box model of the Strait of Georgia—Juan de Fuca system, incorporating a physical parameterization of exchange as a function of along channel density gradients. Babson et al. (2006) used a similar dynamical approach in a box model of Puget Sound. A novel two-tracer approach to diagnosing the exchange flow and mixing, applied to parts of the Salish Sea, is presented in R. Pawlowicz (2001).

Realistic models of the Salish Sea were also attempted in past decades but were significantly hampered by lack of computing power. Modern, realistic models of the Salish Sea only appeared in the last decade (Khangaonkar et al., 2017; Khangaonkar et al., 2011; Moore et al., 2015; Olson et al., 2020; Peña et al., 2016; Soontiens et al., 2015; D. A. Sutherland et al., 2011). The present model continues this realistic numerical approach.

3. Model Setup and Evaluation

The realistic numerical model used here is created using the Regional Ocean Modeling System (ROMS) (Haidvogel et al., 2000; Shchepetkin & McWilliams, 2005) which integrates the Reynolds averaged, Boussinesq, incompressible equations of motion and tracer concentration on a rotating, spherical grid. The model configuration used here is called LiveOcean. The model domain covers all of Oregon, Washington, and Vancouver Island coastal waters, and the Salish Sea—the name for the combined inland waters of Puget Sound, Strait of Georgia, and the Strait of Juan de Fuca (Figure 1). The model grid follows lines of constant longitude and latitude, with 500 m spacing in most of the Salish Sea and Washington coastal estuaries, stretching up to 3 km at open boundaries. There are 30 vertical levels, following the bathymetry and free surface. The model is configured to be as realistic as possible, with 45 rivers, 8 tidal constituents, open ocean conditions from a global data-assimilative model, and high-resolution atmospheric forcing from a regional weather forecast model. The model builds upon prior realistic configurations focused inside of the Salish Sea (D. A. Sutherland et al., 2011) and on the open coast (Giddings et al., 2014). Details of the model setup are given in Text S1. The model run analyzed here was initialized December 15, 2016 and runs through the present because it makes quasi-operational daily forecasts. Here we work only with the three-year period 2017–2019. During 2019, the Salish Sea experienced low river flows (Figure 1c) causing the system to grow progressively saltier.

The three-year model hindcast has been extensively compared to observations. A summary of those comparisons is presented in Supplementary Text S2. Focusing on one aspect of the evaluation most relevant to the exchange flow, along-channel sections of the salinity for 2017 are plotted in Figure 2. Here we use the cast data averaged over the upper and lower parts of the water column at CTD stations to test the model skill at reproducing the along-channel salinity gradient and stratification. The along-channel salinity gradient is thought to provide the driving pressure gradient for the estuarine exchange flow (Giddings & MacCready, 2017; MacCready & Geyer, 2010) and the size of the exchange flow as estimated from Knudsen's Relations depends critically on the stratification. Evaluating these for the three Puget Sound along-channel sections shown in Figure 2 we find that the model salinity gradient is somewhat too weak, being 78%–85% of that observed. The model stratification is 64%–116% of that observed, with the lower value representative of model performance in Hood Canal. The stratification results are most easily related to the exchange flow because the Knudsen's Relations state that the exchange flow is inversely proportional to the stratification (Burchard et al., 2018), so this range suggests our exchange transports may be overestimated by as much as 56% or underestimated by as much as 14%. As mentioned in Supplementary Text S2, there was a significant temporal increase of salinity in the Salish Sea: 0.68 g kg^{-1} over 3 years estimated from CTD data. Comparing to these data, the salinity bias of the model for stations inside Puget Sound stayed roughly the same in each year (0.62, 0.60, and 0.53) implying that the modeled salinity drift was capturing a real trend, and not a spurious model artifact.

4. Calculation of the Exchange Flow and Mixing

The analysis of modeled circulation in the Salish Sea is done in three steps. Our focus will be on subtidal and longer timescales, and on how the exchange flow and mixing affect residence times and tracer con-

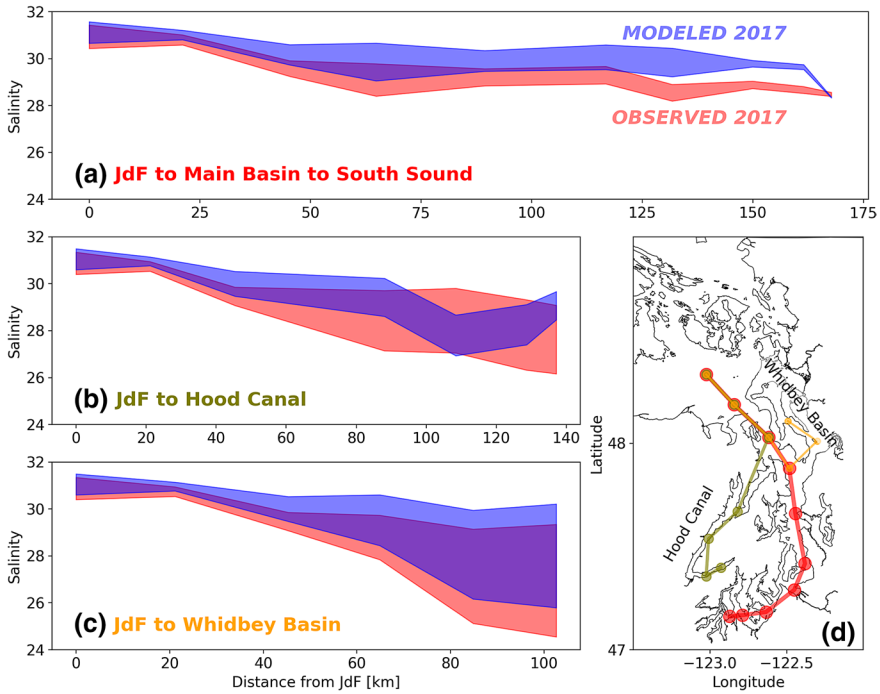

Figure 2. Along-channel salinity distribution calculated from 2017 annual-average salinity using monthly CTD casts (OBSERVED: red) and corresponding model fields (MODELED: blue). The vertical thickness of each line expresses the average stratification: the upper and lower limits are the salinity averaged below and above a chosen depth. The section down Main Basin (a) used 20 m for the chosen depth, while (b) and (c) used 10 m because Hood Canal and Whidbey Basin are more strongly stratified than Main Basin. Station locations are plotted in (d). The colored lines in (d) are the transects shown in (a)–(c).

centrations in general. In the first step, we calculate the tidally averaged exchange flow, following methods described in MacCready (2011), through many sections (Figure 3). Second, we make seasonal and annual averages of the two-layer exchange flow and use these to calculate vertical mixing rates throughout the system. Finally, we use the overall pattern of horizontal transports (the exchange flow) and vertical transports (mixing) to construct an efficient box model of the Salish Sea. The box model is used to explore residence times in different years and seasons. The box model is also used to calculate the concentration and age of a tracer injected from various sources such as a river.

4.1. The Total Exchange Flow (TEF)

The exchange flow is calculated at 39 cross-sections throughout the Salish Sea (Figure 3). At each section, we extract hourly snapshots of section-normal transport and salinity in each grid cell. The sections are aligned with the model grid and located on velocity points of the ROMS C-grid, e.g. for a N-S section such as *jdf1* the cross section is on the model u-grid. Keeping the sections on the model grid minimizes interpolation errors (MacCready, 2011). The 3-year average error in the system-wide volume budget is 0.42% of the average net river flow, and the error in the salt budget is 0.016% of the average salt flux of the inward exchange flow. The largest error found was 2.44% for the Hood Canal 2018 volume budget. For any budget calculations it is essential that volume be conserved as well as possible since any errors in volume transport will propagate through all tracer transport calculations. Comparing the error to mean river flow in a basin, as we do here, is a conservative approach because typically the exchange flow transports are an order of magnitude larger.

The exchange flow is calculated at each section using the TEF method (MacCready, 2011). Here transport is sorted into salinity classes, tidally averaged and then the sum of the transport in all inward flowing salinity classes is called Q_{in}. The flux-weighted salinity of the inflow is S_{in}. Similarly, the out-

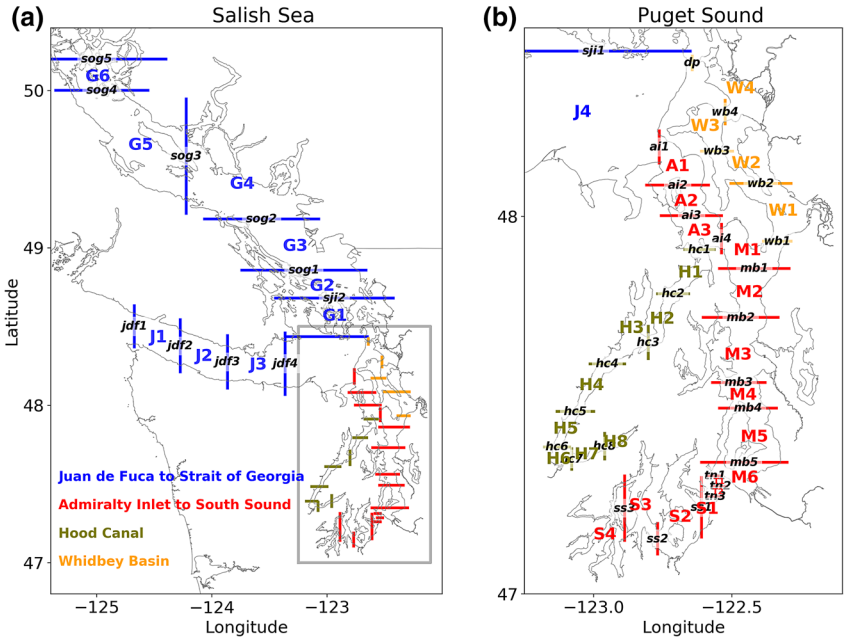

Figure 3. Sections used for the TEF analysis in the Salish Sea (a). Sections are shown as lines and lower-case names like *jdf1*. A close up of Puget Sound sections is shown in (b). The names of segments (the volumes in-between sections) such as J1 are also shown. Segment letters denote the following basins or sills in Puget Sound (b): A, Admiralty Inlet; H, Hood Canal; M, Main Basin; T, Tacoma Narrows; S, South Sound; W, Whidbey Basin. In the larger Salish Sea (a) J, Strait of Juan de Fuca; G, Strait of Georgia. Section *sog5* at the top of (a) is the start of Johnstone Strait which is a minor connection between the Strait of Georgia and the Pacific Ocean. Section *dp* near the top of (b) is Deception Pass which connects the north end of Whidbey Basin to the eastern Strait of Juan de Fuca. The sections *tn1*, *tn2*, and *tn3* in (b) are at Tacoma Narrows which connects South Sound to Main Basin. TEF, total exchange flow.

flow is quantified as Q_{out} and S_{out}. The sign convention is that Q_{out} is negative. These TEF variables thus consist of four tidally averaged time series at each section. The reason for using salinity classes is that it accounts for tidal variation in the spatial structure of the salt flux (MacCready, 2011). The TEF variables give the total inward and outward salt flux through a section as $Q_{\text{in}}S_{\text{in}} + Q_{\text{out}}S_{\text{out}}$ regardless of whether the salt flux was due to steady exchange flow or tidal pumping. TEF has been found to give a clear representation of the exchange flow in many systems (Burchard et al., 2018; Chen et al., 2012; Conroy et al., 2020; Geyer & MacCready, 2014; Lorenz et al., 2020; Rayson et al., 2017; D. A. Sutherland et al., 2011). Using the TEF method is especially appropriate in the Salish Sea because the system is known to have large basins with exchange organized by depth (deep saltier inflow, shallow fresher outflow) punctuated by energetic sills like Tacoma Narrows where the exchange is organized by time (saltier flood, fresher ebb).

We calculate transport in 1,000 salinity bins and then integrate over these to form inflowing and outflowing layers using the "dividing salinity" method (MacCready et al., 2018) which has been shown to give reliable results even for nearly well-mixed cases (Lorenz et al., 2019). We allow for the existence of more than two layers in calculating our initial layer averages (Lorenz et al., 2019), but then combine these into just two layers, conserving net salt flux in either direction. An example of the results is plotted as time series for section *ai3* in Figure 4. At this section, there is a clear annual cycle of the salinity of the two layers, growing saltier and with less salinity difference between in- and outflow in the late fall when river flows have been low for some months. The daily values show evidence of increased salinity of the inflow during weak neap tides (Figure 4a), consistent with the observations of Geyer and Cannon (1982). The exchange flow transport (Figure 4b) also shows annual and fortnightly variation. The dynamics controlling these is of great importance but will not be addressed in this paper because we are focusing instead on describing the circulation and its implications for residence time. About half of the sections could be characterized as having more than two layers at times, and this is an important caveat on our subsequent calculations

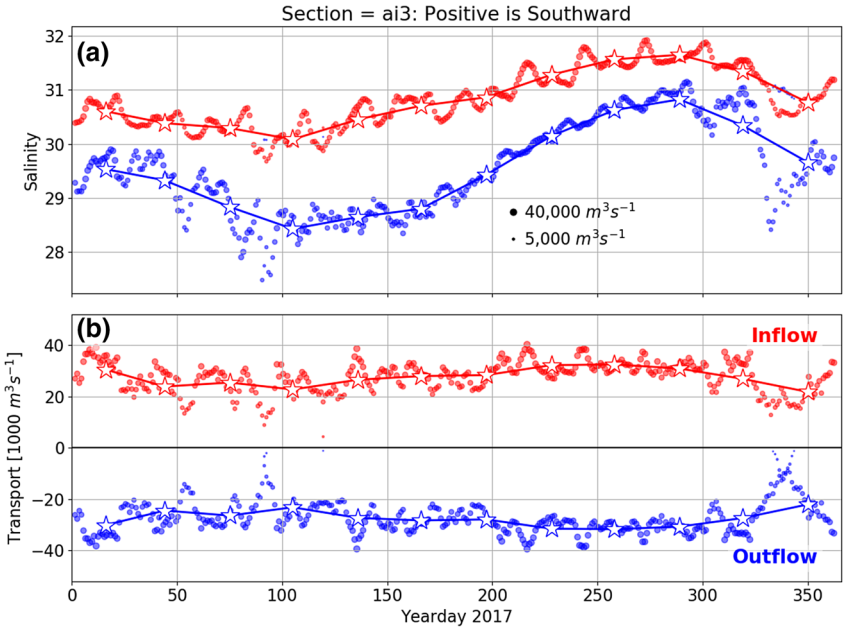

Figure 4. TEF salinity and (b) transport at section *ai3* in Admiralty Inlet plotted versus yearday for 2017. The red and blue dots show tidally averaged daily salinity or transport from the multi-layer TEF analysis. Dot size is proportional to transport. The monthly averaged two-layer TEF terms S_{in}, S_{out} and Q_{in}, Q_{out} are shown as stars connected by lines.

using transports that have been expressed somewhat artificially as two layers. A more nuanced approach allowing three or four layers is presented in Pawlowicz et al. (2007) for the Strait of Georgia. We proceed by assuming that a two-layer estuarine circulation is adequate for understanding the broad patterns of circulation in the Salish Sea, but caution that the details of stratification and water residence time in a given basin are best handled by calculations using a realistic model, albeit at substantially greater computing cost.

The two-layer transports for all sections averaged over 2017 are plotted in Figure 5. In general, the magnitude of the exchange flow transport increases steadily moving seaward. However, the increase is not perfectly monotonic, e.g. between sections *tn2* and *tn3* at Tacoma Narrows (Figure 5b). This is consistent with previous results (D. A. Sutherland et al., 2011) that also used the TEF method. The results are inconsistent with the characterization of the Salish Sea circulation presented in Ebbesmeyer and Barnes (1980) and Khangaonkar et al. (2017) which did not use the TEF method. The places where our results differ most is at the sills, with the exchange flow in Khangaonkar et al. (2017) at Admiralty Inlet being about half what we find, and that in Tacoma Narrows being about one tenth of what we find. This is not to say that the Khangaonkar et al. (2017) model is incorrect; indeed it has circulation patterns and validation statistics that are similar to what we present here. The difference is that the TEF method is required to correctly quantify the exchange flow at energetic places like sills where salt flux due to tidal pumping may be an important mechanism. This is because at sills there is local enhancement of tidal currents and often distortions of the salinity field due to rough bathymetry that may lead to local tidal correlation of salinity and transport (i.e. tidal pumping). The TEF method, by construction, includes tidal pumping as part of the net advective flux. This distinction is important for our understanding of the circulation of the Salish Sea. In Ebbesmeyer and Barnes (1980), the circulation was described as a two layer flow that was interrupted at sills, with the seaward-flowing surface layer being largely sent downward by refluxing at a sill, resulting in a conceptual model in which the basins were much more isolated from each other than our calculations suggest. Nonetheless, there is a lot of vertical mixing and refluxing of water at sills, but it does not interrupt the horizontal exchange flow in the way envisioned by previous authors. We explore this distinction further below. More TEF section results are given in the Text S3, showing patterns of tidal energy flux and net volume transport.

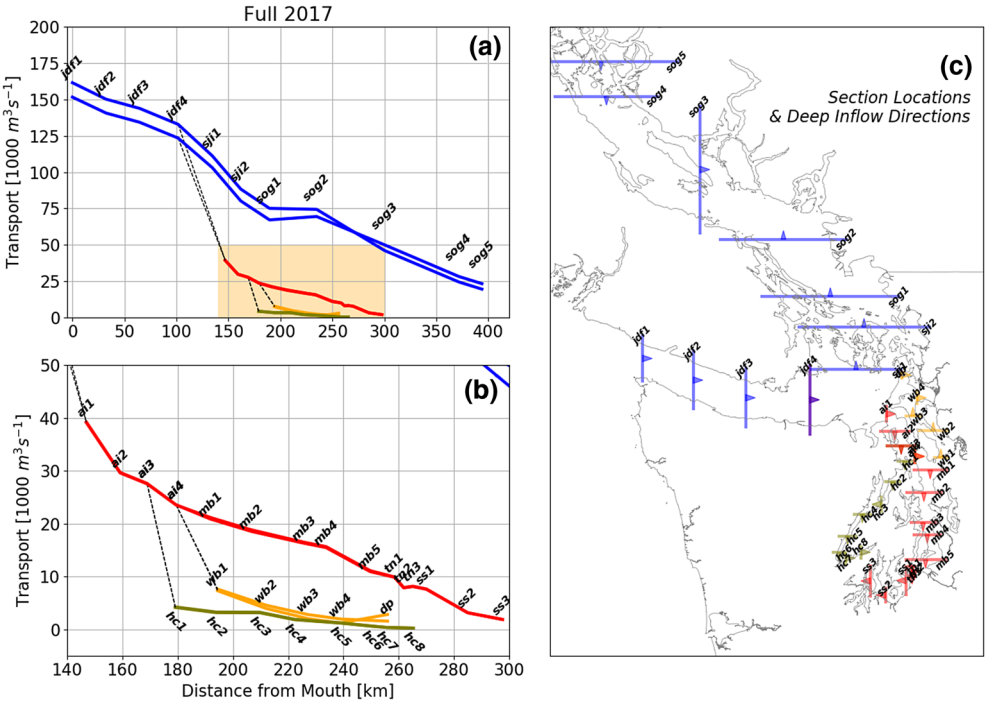

Figure 5. Total Exchange Flow volume transports averaged over 2017 for the four main channels of the Salish Sea (a). The lines are Q_{in} and $-Q_{out}$, so the higher of the two blue lines in (a) is the outflow. An expanded view of Puget Sound transports is plotted in (b). Section locations and names are shown in (c) with the spike on each section line showing the direction of the deep inflow. Note that the exchange flow reverses sign in the Strait of Georgia between sections *sog2* and *sog3*. The dashed lines at the seaward end of basins, e.g. from *hc1* to *ai3* in (b) indicate connections between the channels.

The TEF properties are a compact way to represent the system behavior. A three-year time series of S_{in} and S_{out} for the Puget Sound sub-volume (with bounding sections at *ai1* and *dp*) is plotted in Figure 6a. Also plotted is the volume-mean salinity over that time period, which increases by about 0.7 g kg^{-1} while the salinity difference between inflow and outflow, $\Delta S \equiv S_{\text{in}} - S_{\text{out}}$, decreases. The exchange flow over that time did not exhibit a clear multi-year trend (Figure 6b), although it does have a strong annual cycle, peaking in winter when the river flow (Figure 6d) is strong. The annual mean river flows entering Puget Sound were close to average in 2017, dropped a bit in 2018, and dropped by a third in 2019 (Figure 6d). Similar budgets (not shown) were formed for other sub-volumes of the Salish Sea, and for the complete system, and in all cases the salinities had a sensible relationship to the net river flow: during times of low flow like the late summer or 2019, the salinity was increasing and ΔS was decreasing. The exchange flow, in contrast, was much harder to explain. There was no consistent phasing between exchange flow and net river flow, nor was there an interannual trend. This may represent the unusual plumbing of the system. Taking the Puget Sound volume (Figure 6) as an example, the biggest freshwater source in the Salish Sea is seaward of Puget Sound and peaks some months later than Puget Sound Rivers (Figure 1). The exchange flow may also be influenced by the density of water upwelled on the coast during spring and summer (Babson et al., 2006), the seasonal variation of wind (D. A. Sutherland et al., 2011), and tides (Deppe et al., 2018).

A complete salt budget may be formed from the TEF quantities, and the terms may be expressed most clearly by defining an exchange flow transport Q_e as the average of Q_{in} and $-Q_{\text{out}}$ (recall Q_{out} is defined as negative). We also define an average salinity of the exchange as $\overline{S}$, and the net river flow entering a volume as Q_R (defined as positive).

$$Q_e \equiv \frac{(Q_{\text{in}} - Q_{\text{out}})}{2}, \tag{1}$$

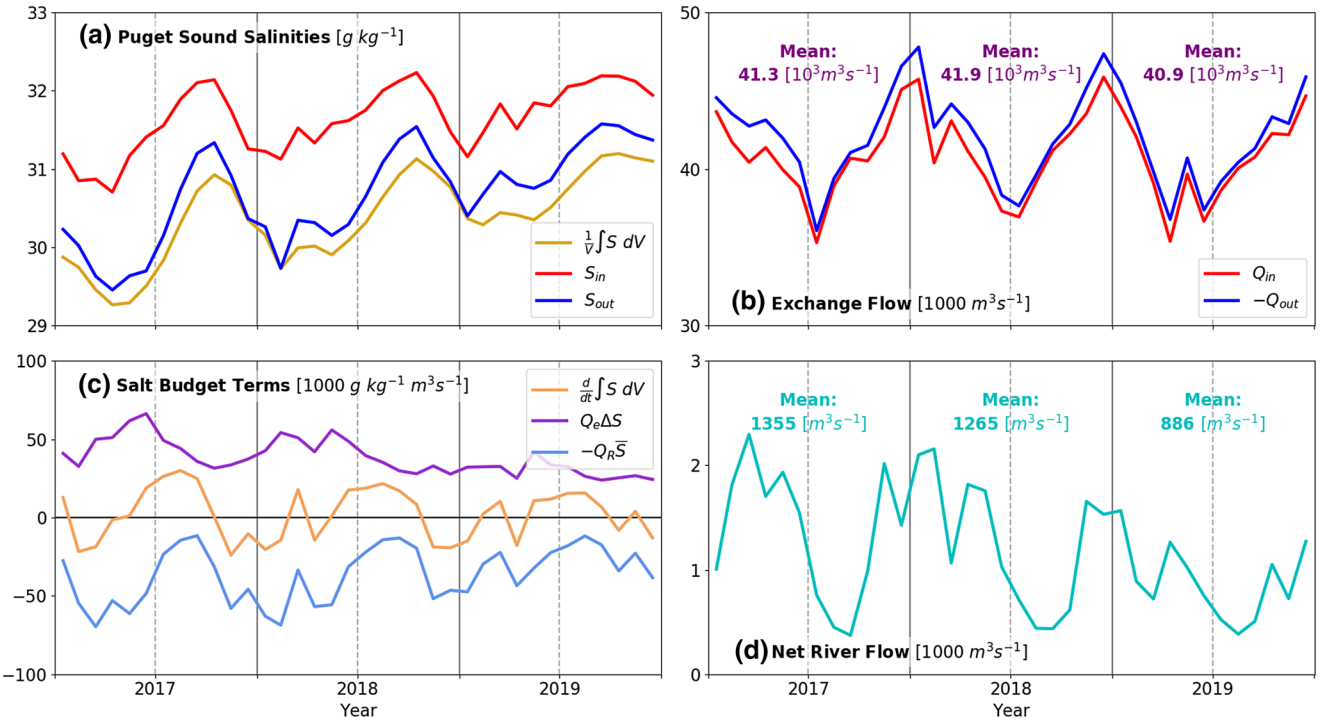

Figure 6. Three-year TEF analysis time series for Puget Sound salinity. The bounding sections for the volume are *ai1* and *dp*. Salinities of the in- and outflow are plotted in (a) along with the mean salinity in the volume. The term $V^{-1}\int S\,\mathrm{d}V$ is lower than S_{in} and S_{out} because is it the average over the whole volume of Puget Sound, not the average of S_{in} and S_{out}. All values are monthly averages. The exchange flow transports are plotted in (b) with annual means shown for each year as text. Terms in the exchange flow salt budget are plotted in (c). The net river flow is plotted in (d) with annual means shown for each year as text. Year labels are at the middle of the year.

$$\overline{S} \equiv \frac{\left(S_{\mathrm{in}} + S_{\mathrm{out}}\right)}{2}. \tag{2}$$

Then the tidally averaged, volume-integrated salt budget may be written in two ways:

$$\frac{\mathrm{d}}{\mathrm{d}t}\int S\,\mathrm{d}V = Q_{\mathrm{in}}S_{\mathrm{in}} + Q_{\mathrm{out}}S_{\mathrm{out}}, \tag{3}$$

$$\frac{\mathrm{d}}{\mathrm{d}t}\int S\,\mathrm{d}V = -Q_R\overline{S} + Q_e\Delta S. \tag{4}$$

The terms on the right-hand side of (4) are the TEF equivalent of the classic estuarine salt budget, e.g. Equation 10 in MacCready and Geyer (2010), but without the need for a tidal pumping term. Physically, the net river flow removes salt, and the exchange flow brings salt in. The terms in (4) are plotted in Figure 6c. The gradual decrease of the exchange term, $Q_e\Delta S$, over time is driven by the decrease in stratification, ΔS, but this was more than matched by the decreasing magnitude of the river term, leading to the increase of mean salinity.

4.2. Efflux-Reflux Fractions and a Box Model

From the time-mean TEF two-layer transports and salinities we may also determine the net vertical mixing in any segment between TEF sections. The method was first developed in Cokelet and Stewart (1985) and was applied to Puget Sound in a series of NOAA reports and one conference paper (Cokelet et al., 1991). What the efflux-reflux formalism does is to split the turbulent transport into independent upward and downward components. The advantage of doing so is that it expresses the vertical fluxes as volume transports, making

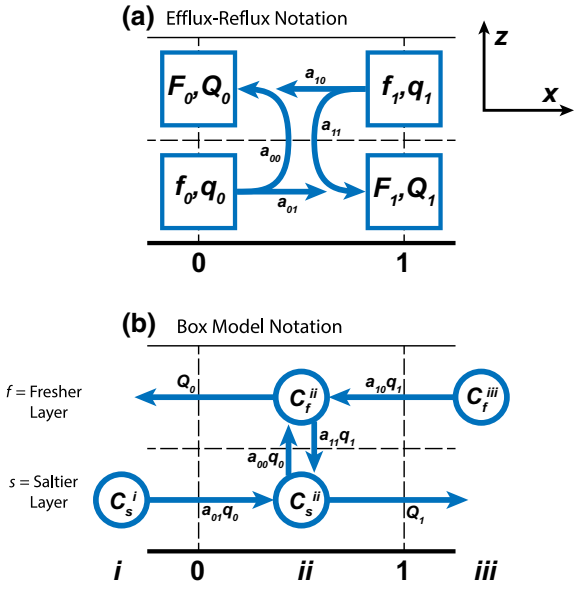

Figure 7. Sketch of notations used for (a) the efflux-reflux calculations, and (b) the box model. Each panel represents three segments (*i*-*iii*) divided by sections 0 and 1. Each segment has two layers in the vertical, a deep saltier one and a shallow fresher one. TEF volume and salt fluxes are denoted by Q, q, and F, f in (a), and the efflux-reflux fractions are a_{00} and so on ($a_{\text{from,to}}$). In the box model (b) C denotes the concentration of an arbitrary tracer, and the subscripts f and s denote the "vertical" delineation.

them the vertical equivalent of the horizontal TEF fluxes. The advantage of using the TEF transports is that they are the complete terms which allow (3) to be satisfied, in the same way that they satisfy the Knudsen's relations (Burchard et al., 2018; MacCready, 2011), without the need for fluxes due to tidal pumping, which may not be separated by layer. The existence of realistic numerical simulations, as used here, and the TEF calculation method, represent the main advances in the tools we may use with the efflux-reflux theory. The fact that these tools were not available to Cokelet and Stewart (1985) motivates our effort here to revisit Salish Sea circulation and mixing.

Here we extend their method to the entire Salish Sea for multiple years and seasons and use it to construct an efficient box model to calculate residence times for different basins, seasons, and definitions of the residence time (see below). In its simplest form, the efflux-reflux theory can be applied to a single channel segment between two sections with no river input (Figure 7a). The segment is assumed to have two layers and known, steady, volume and salt transports through the open sections on either side. Because of the complexity of applying this to many segments in a complex geometry like the Salish Sea, we define a local notation in which all transports are positive, inflows are lower case (q or f) and outflows upper case (Q or F). In standard TEF notation q would be Q_{in}, and f would be $Q_{\text{in}}S_{\text{in}}$, the inward salt flux. The efflux-reflux theory determines what fraction of the deep (saltier) flow entering the segment must be mixed or advected into the upper (fresher) flow leaving the segment, and this is called "efflux." Likewise, the theory determines what fraction of the fresher flow entering the segment must be mixed or advected down into the saltier flow leaving the segment. The fraction is called "reflux" because in a typical estuarine channel it represents seaward-flowing surface water being mixed down and pulled back landward. The importance of reflux is that it can retain tracers in the system, increasing residence time. The theory determines the efflux-reflux fractions under the dual constraints of volume and salt conservation, as detailed in Cokelet and Stewart (1985). The system of equations to be solved for the segment shown in Figure 7a are, in matrix form:

$$\begin{bmatrix} q_0 & q_1 & 0 & 0 \\ f_0 & f_1 & 0 & 0 \\ 0 & 0 & q_0 & q_1 \\ 0 & 0 & f_0 & f_1 \end{bmatrix} \begin{bmatrix} a_{00} \\ a_{10} \\ a_{01} \\ a_{11} \end{bmatrix} = \begin{bmatrix} Q_0 \\ F_0 \\ Q_1 \\ F_1 \end{bmatrix}. \tag{5}$$

The four unknown coefficients, $a_{\text{from,to}}$, are then determined by standard matrix techniques. The existence of a solution requires that volume and salt be conserved, e.g. for salt flux:

$$f_0 + f_1 = F_0 + F_1, \tag{6}$$

And the fractions must be positive and sum to 1, e.g. $a_{00}+a_{01} = 1$. The efflux and reflux could also be expressed in more familiar form as the sum of vertical advective transport and vertical turbulent transport. Vertical turbulent transport is physically caused by the net effect of upward and downward advection of water parcels, and in the formalism used here we keep track of up and down transports separately.

As pointed out at great length by Cokelet and Stewart (1985) there are many real-world complications to applying the theory to complex systems such as the Salish Sea. Chief among these is that for segments with rivers (e.g. W4) or with more than two bounding sections (e.g. J4) the resulting system of equations is underdetermined. For these cases we take a pragmatic, numerical approach, making many guesses for some of the a's and then using the average of all physically possible solutions. In the rare cases with no solutions we

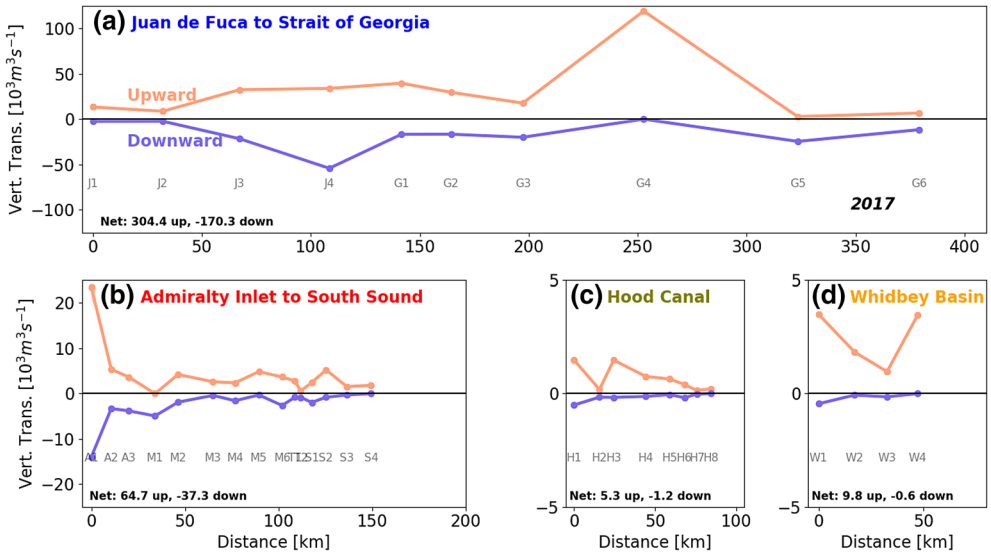

Figure 8. Vertical transports in segments for each channel from the efflux-reflux box model. Values shown are for the full year 2017. In each segment, there may be both upward and downward transports, which is an alternate way of quantifying the effects of vertical advection and mixing. Note that the *y*-axis scales change for each panel. The sum of all up or down transports in each channel is shown in text at the lower left (10^3 m^3s^{-1}).

impose a typical value of 0.1 to the reflux coefficients (a_{00}, a_{11}, and so on). In one segment, A1, we adjusted the reflux fractions by hand to achieve a better result. To ensure exact volume and salt conservation, we make very small adjustments (at most 0.5% and usually much smaller) to the fluxes bounding each segment before calculating the fractions. The lack of perfect conservation is due in part to the fact that the volume and salt budgets are not exact, as discussed above. In addition, the net salt in a segment may be changing over time, and this unsteadiness is neglected because it is small compared to the other fluxes. Nonetheless we capture some aspects of temporal variability by calculating the efflux-reflux fractions over different years and seasons.

We then use the TEF transports and efflux-reflux fractions to create a box model for arbitrary tracers, as shown schematically in Figure 7b. Each segment is composed of two volumes, with the upper (fresher) volume being 20% of the total in a given segment—an approximation of the observed structure of the Salish Sea. The residence time results presented below are not particularly sensitive to this choice, varying by only ±7% when the upper volume was 10% or 30% of the total in a segment. The concentration of an arbitrary tracer in each volume is given by C, which can be time-dependent even though the circulation is steady. We take all the "reflux" parts of the efflux-reflux calculation and use them to determine upward and downward transports vertically between fresher and saltier volumes in a segment. Following the arrows and notation in Figure 7b, the equation for tracer concentration in the fresher volume of the segment is:

$$\frac{dC_f^{ii}}{dt} = C_f^{iii} q_1 (1 - a_{11}) + C_s^{ii} q_0 a_{00} - C_f^{ii} Q_0 . \tag{7}$$

In segments with more than two surrounding sections, the vertical transports are formed by the sum of all the reflux terms. An example of the resulting upward and downward transports for the full year 2017 is plotted in Figure 8. If they are equal in magnitude that means that there is vertical mixing but no mean vertical flow in a segment. In general, in Figure 8, it is apparent that upward fluxes are usually larger than downward, implying that the mean transport is upward, consistent with conceptual sketches of estuarine circulation as in MacCready and Geyer (2010) (their Figure 1a). The net up and down transports in each channel are given as text in Figure 8. Notably, the net upward flow is generally larger than the exchange flow at the seaward end of a channel (see Figure 5) because it must accommodate both the transformation of inflow to outflow and the vertical mixing. Numerically, the box model integrates 37 × 2 equations such as (7) using forward time-stepping and a time step of 1 hour (chosen for numerical stability). Had we plotted the

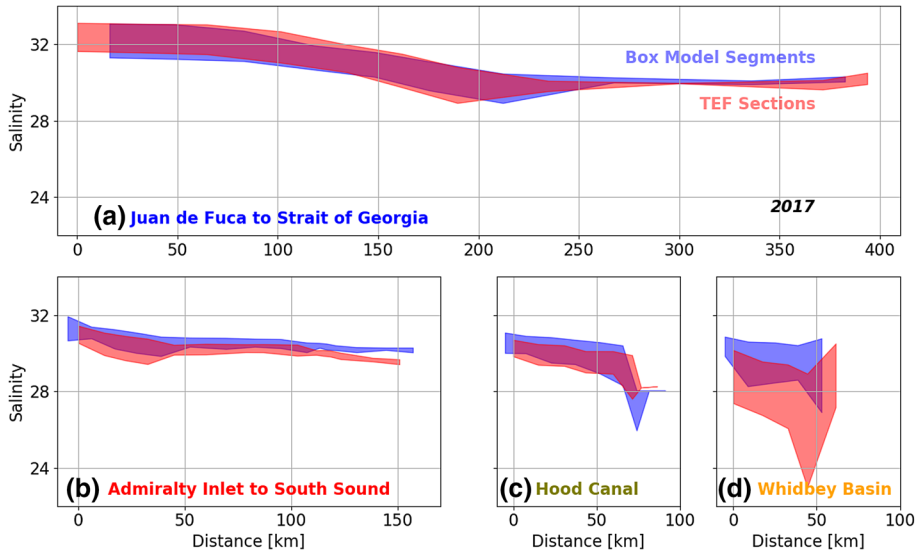

Figure 9. Test of the ability of the box model to reproduce the TEF salinities that were used to construct it. Each panel is for one of the four channels of the Salish Sea, and shows the range between upper- and lower-layer salinities as the vertical line thickness, versus along channel distance. For the box model, these salinities are in the segments, whereas for the TEF sections, they are S_{out} and S_{in} on the sections.

transports as vertical velocities (i.e. dividing by the horizontal area of each segment) the sills would show the largest values, but the area integrals in Figure 8 demonstrate that mixing in basins cannot be neglected.

The resulting box model of the Salish Sea can be tested by seeing how well it reproduces the TEF salinities when the boundary conditions are $C = 0$ for all the rivers and $C = S_{in}$ at the two open ocean boundaries. Results of this test for the full year 2017 are plotted in Figure 9. Overall the box model does a reasonable job of reproducing the along-channel gradient and stratification (S_{in}—S_{out}) throughout the system. The model results are biased high in the three channels of Puget Sound, however, and the model underestimates the stratification in Whidbey Basin. Experiments with the box model in an idealized estuary (not shown) suggest that some of the error may be due to the relatively coarse spatial resolution of the boxes. It is also possible that different choices of efflux-reflux fractions in specific segments might improve the model. With its imperfections in mind, we take the box model to be good enough for our purposes of exploring residence times and other properties.

We perform two types of experiments with the box model. In the first, we introduce a steady input of tracer with concentration $C = 1$ at a selected river or rivers. We call these "source experiments." The integration is run out to equilibrium (6 years—empirically found to be long enough) and a result consists of the steady-state tracer concentration in each segment, both upper and lower sub-volumes. We also run a tracer with the same boundary conditions but which grows at a known rate, and use the ratio of the two tracers to estimate the "age" of the tracer since it was introduced (e.g. from a river), as discussed for example in Rayson et al. (2016).

In the second type of experiment, the tracer is introduced as an initial condition with $C = 1$ in a volume V composed of selected segments. We will call these "initial condition experiments." We present results from experiments of this type in seven different basins of the Salish Sea and for different time periods.

The concept of residence time has been used in many different ways as discussed for example in Monsen et al. (2002), Delhez et al. (2004), and Lemagie and Lerczak (2015). Usually the motivating question is water quality, e.g. hypoxia, and the time water spends in a region is just one of several driving factors. Residence time is also greatly influenced by how it is defined. Here we adopt the definition that the residence time, T_{res}, is defined through an initial condition experiment: (i) we choose a volume to focus on—e.g. all the water in Puget Sound, (ii) we introduce a conservative tracer with concentration $C = 1$ in that volume at some time,

and $C = 0$ elsewhere, (iii) we allow advection and mixing to move the tracer around, and then (iv) calculate T_{res} as the time after the start when the integrated tracer concentration in the volume drops to 1/e or about 37% of its original value. We recognize that formally "residence time" is defined for each water parcel (Monsen et al., 2002) and so is a function of space and time. Our T_{res} amounts to an average that describes the behavior of a collection of water parcels, and is analogous to what has variously been called the system residence time, turnover time, or particle tracking timescale.

For most of our experiments T_{res} is influenced by reflux: some of the water expelled from a channel by the outgoing branch of the exchange flow may be mixed down outside of the volume under consideration and be returned to the volume by the incoming branch of the exchange flow. The box model described above is an efficient platform for doing such calculations, taking just seconds for a 6-years integration. We may also define an alternate exchange flow, T_{resNX}, which is the "residence time without reflux." It is also calculated from initial condition experiments, but with different rules: instead of allowing the tracer to freely flow and reflux throughout the system, we set $C = 0$ at all times outside of the volume in which the tracer was initialized. A third, and much more common, way to calculate a timescale is as the "flushing time," defined as $T_{flush} = V/Q$ where V is the size of the volume being considered and Q is the water flux through the volume. In our case we take Q to be the sum of all the $-Q_{out}$, which is equivalent to the sum of all the Q_{in} and the river flows. If the tracer is continuously homogenized within a volume, then it is straightforward to prove that $T_{flush} = T_{resNX}$. However, in general, the tracer is not homogenized – some segments of the volume are flushed faster than others, and this lack of homogeneity generally causes $T_{flush} < T_{resNX}$. By calculating all three timescales from our box model experiments we may quantify the relative importance of reflux and lack of homogenization which lead to T_{res} being greater than T_{flush}.

We computed TEF transports and vertical efflux-reflux transports for all segments for 15 cases: averages over each of the 3 years 2017–2019, and the four seasons in each year, defined as averages over three months in a given year: winter = JFM, spring = AMJ, summer = JAS, fall = OND. The transports used in the box model in each case are steady, the result of averaging the full time-varying transports over the time interval in question. When the box model is run for a given case it is different from the real system in the sense that a given circulation pattern and river flow are maintained for much longer than three months or a year, so one can think of the experiments as answering the hypothetical question: what would the residence time be under these conditions if they persisted?

5. Results from the Box Model

An example from a source experiment in which the source was all the rivers in the Salish Sea is shown in Figure 10, with forcing from 2017, a year with average river flow. Notable results are that river water rarely makes up more than 15% of a sub-volume; and only 8% in the main basin of Puget Sound. The age of the water is on the order of 200–300 days, longer in the Strait of Georgia and shorter in Puget Sound. The age represents the combination of transport pathways of many rivers, however, and may be greatly influenced by the system-wide spread of Fraser River water (Banas et al., 2014). The surface concentrations are generally higher (more river influence) and younger.

A snapshot from an initial condition experiment is shown in Figure 11. Here the tracer was initialized in all sub-volumes of South Sound, and then advected and mixed with transports from winter 2019. This was the experiment that had the largest difference between T_{res} and T_{flush}, as discussed below, but it also nicely illustrates the pathways by which a tracer is dispersed throughout the Salish Sea on its way to eventually exiting to the Pacific. In particular, while tracer heads seaward in surface layers, it is also mixed (refluxed) downward, and may thereby drift into other basins, following the deep inflow. This is apparent in all of the channels in Figure 11.

Residence times were calculated from initial condition experiments with dye initialized in seven different basins (Figure 12 and Table 1). 12 experiments were done in each basin, comprised of 3 years and four seasons in each year.

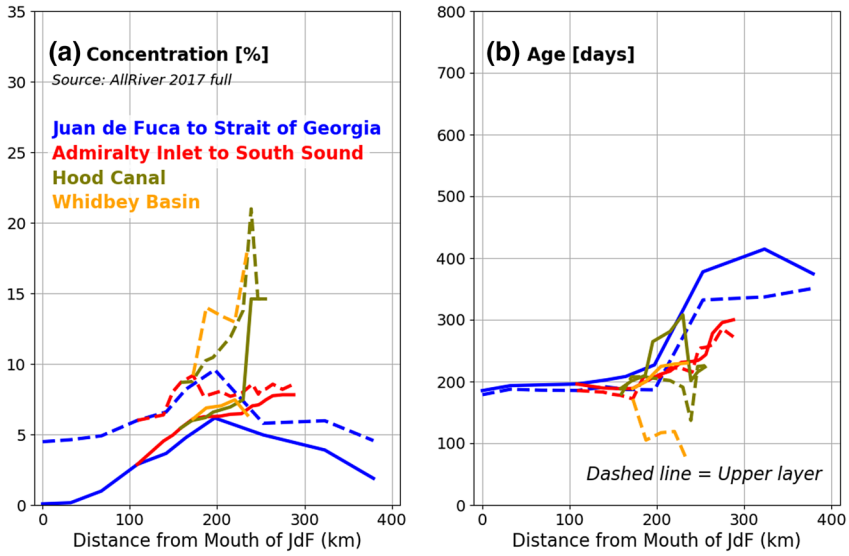

Figure 10. Result for the final state of a box model source experiment with a tracer of concentration one coming out of all the rivers. The circulation, mixing, and river flows are assumed to have the values of the mean of 2017 for the entire 6-year integration. Final concentration is shown in (a) and age in (b). The solid lines are the bottom sub-volumes of each segment, and the dashed lines are for the surface sub-volumes.

For the full Salish Sea (all of the segments in Figure 3a), the average residence time is almost a year and is shortest in summer when the circulation is most affected by the large pulse of freshwater delivered by the Fraser River (Figure 12). Residence times increased by about 50 days over the 3 years studied, presumably a result of the weaker river flow in 2019. The flushing time is less than half the residence time, and the difference is due to lack of complete homogenization within the volume. The other possible explanation, reflux, cannot affect this case because the tracer leaving the box model does not come back so $T_{\mathrm{resNX}} = T_{\mathrm{res}}$ in this case (Figure 12).

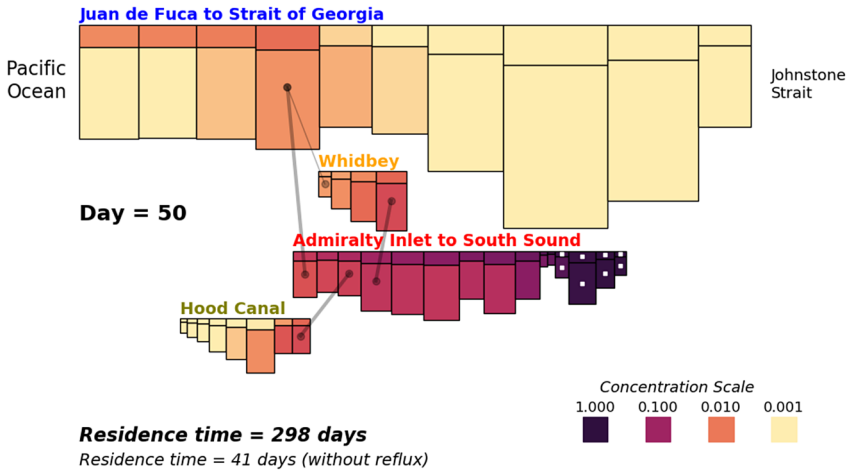

Figure 11. Snapshot of a time-dependent integration of a box model experiment in which there is a tracer initial condition, but no tracer coming in from the river or ocean sources. In this case, the tracer was set to one in the volumes of South Sound (dark color with white squares) and allowed to advect and mix at rates from winter 2019. The snapshot is from 50 days into the integration, with color indicating $\log_{10}$ of the concentration. Each segment is shown as a rectangle (divided into upper and lower sub-volumes) and the rectangle size is proportional to segment volume. Connections between channels are shown as gray lines—the thin gray line connecting Whidbey Basin to the Strait of Juan de Fuca is Deception Pass.

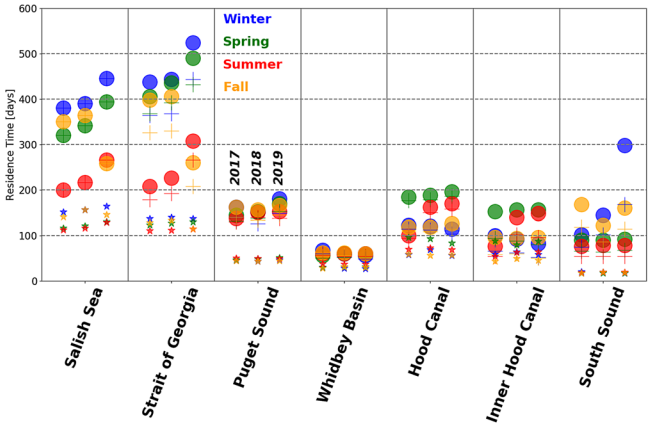

Figure 12. Residence times from box model initial condition experiments for various basins in four seasons (colors). Each basin has values for three different years (separated horizontally as indicated for Puget Sound). The large filled circles are T_{res}, the residence times calculated from the box model as the *e*-folding time of a tracer initialized with concentration one in the segments of that basin and 0 elsewhere. The smaller stars are T_{flush}. The crosses are T_{resNX}. The Hood Canal Inner volume consists of just the deeper portions of segments H3-H8.

Turning to the Strait of Georgia, the residence times are somewhat higher while the flushing times are slightly lower. The longer residence times reflect the fact that deep Strait of Georgia takes a long time to lose its tracer due to its large volume. The effect of reflux is evident in that $T_{resNX} < T_{res}$. From this difference we may calculate the fractional effect of reflux:

$$f_{reflux} = 100 * \frac{(T_{res} - T_{resNX})}{(T_{res} - T_{flush})}. \quad (8)$$

For this case, the average value is $f_{reflux} = 22\%$ (Table 1), meaning that omitting reflux decreases the residence time relative to the flushing time by 22%. From this we may conclude that most (78%) of the reason that $T_{res} > T_{flush}$ is the lack of complete homogenization of tracer in the volume. Physically, much of the tracer is sequestered in parts of the volume that are flushed slowly, while tracer close to the boundaries is flushed very rapidly.

The average flushing time in the Strait of Georgia volume is found to be 125 days. This may be compared to estimates made by Pawlowicz et al. (2007). They used time series of observations over 3 years, exploiting the annual cycle of water properties and the phase lag of properties inside of the Strait of Georgia compared to those of the primary source water in the Strait of Juan de Fuca. Their analysis recognizes the lack of complete homogenization, but they make assumptions consistent with those of the flushing time given above, so their numbers are most directly comparable to our T_{flush}. They examine four layers, the largest of these is the "intermediate layer" (analogous to most of our deep layer) for which they report a flushing time of 160 days. A volume-weighted average of all their layers gives flushing times of 112 days in summer and 172–319 days in winter. The longer times in winter are due to the extreme range (1–3 years) that they give for the flushing time of the deepest water in the Strait of Georgia, although these are never realized because of summer deep renewal events. These bound our estimated average flushing time. Most striking however, is the fact that our mean residence time, 379 days, is three times longer than our flushing time, and as discussed above, most of the cause for this increase is lack of homogenization in the volume. Rich Pawlowicz et al. (2007) also estimate that ocean water spends about 1.7 years in the Strait of Georgia after accounting for the substantial reflux in Haro Strait that returns outgoing surface waters back as deep waters. In "source" experiments with our box model (not shown), we find ocean water ages of about 1.2 years in the Strait of Georgia. However, there are many different assumptions that go into the two estimates, so they are not exactly comparable. For our results, the 50% uncertainty reported in Rich Pawlowicz et al. (2007) is probably a reasonable estimate as well.

Similar results are evident in Puget Sound and its basins. Previous median flushing times from D. A. Sutherland et al. (2011) are given in Table 1. These are most directly comparable to the T_{flush} presented here because they used a similar numerical model of the Salish Sea and the TEF method of exchange calculations. The only conceptual difference was that D. A. Sutherland et al. (2011) used the saltwater flushing time whereas we use the volume flushing time; these are very similar for volumes that are mostly seawater. Our results are 14%–23% shorter than the previous estimates but display the same pattern among basins: Hood Canal has the longest flushing times, and Whidbey Basin and South Sound are much shorter. As in the Strait of Georgia, the residence times from our box model are markedly longer, being 2–3 or even up to 6 times as long as the

Table 1
Residence and Flushing Times in Days, Averaged Over all Years and Seasons in Each Basin (Figure 12) are Given in the Left Three columns

	T_{res}	T_{resNX}	T_{flush}	f_{reflux}	D. A. Sutherland et al. (2011)	Pawlowicz et al. (2007)
Salish Sea	327	327	136	0%	–	–
Strait of Georgia	379	322	125	22%	–	112–319
Puget Sound	157	138	47	17%	57	–
Whidbey Basin	60	53	31	24%	24	–
Hood Canal	143	134	70	13%	81	–
Hood Canal Inner	116	72	63	83%	–	–
South Sound	125	85	18	37%	21	–

Note. Three different timescales are given, as defined in the text, along with the fraction f_{reflux} by which T_{res} is changed when reflux is not included. Comparisons to selected previous results are shown in the right two columns, as discussed in the text.

flushing time. Again, most of the longer time is explained by lack of homogenization within the volume, with only 13%–37% explained by reflux (Table 1) in most cases.

The exception is the Hood Canal Inner volume which has $f_{reflux} = 83\%$. This experiment differed from the others in that we only initialized tracer in the deeper parts of each segment (H3-H8 in this case). Thus, tracer could be lost rapidly in the no-reflux experiments when it escaped to the upper layer through vertical mixing and advection (i.e. efflux). This result suggests that for a non-conservative tracer which is reset in the upper layer, e.g. by photosynthesis or air-sea gas exchange, the residence time may be closer to the flushing time.

6. Summary and Discussion

In this paper we have presented results from a 3-year hindcast of a realistic numerical simulation of the Salish Sea and adjoining coastal waters of the Northeast Pacific. The model is forced with realistic tides, winds, atmospheric heat fluxes, open ocean conditions, and rivers. Based on extensive validation the model is shown to perform well in reproducing observed fields. The model velocity and salinity fields are then used to calculate the exchange flow from hourly snapshots at many sections, using the TEF method. The exchange flow is strongest at the open boundaries, especially the mouth of the Strait of Juan de Fuca, and is amplified by a factor of 20 or more compared to the net river flow. The strength of the exchange flow decreases gradually, and nearly monotonically, going landward. This implies that the many basins of the Salish Sea are intrinsically connected to each other by this exchange flow.

The vertical mixing throughout the system was quantified using the efflux-reflux method of Cokelet and Stewart (1985). In this formalism, vertical mixing and advection are expressed as opposing upward and downward volume fluxes, analogous to the horizontal TEF fluxes. Notably the downward fluxes highlight the many places where the outward flowing surface layer is refluxed into the landward-flowing deep layer, fundamentally shaping the tracer transport pathways. Low river flow in 2019 resulted in a clear increase of salinity in Puget Sound, and a decrease in stratification, but no obvious change to the exchange flow. Nevertheless, residence times were longer in 2019 compared to 2017–2018. A box model for tracer transport was developed using these horizontal and vertical fluxes, with transports from four seasons in each of 3 years. The box model allowed rapid calculation of residence times for a number of sub-volumes. In general, it was found that the tracer-based residence time from the box model was often a factor of two longer than the more traditional calculation of flushing time. The increase was due in part to refluxing which brings tracer back into a volume, but in larger measure the increase was due to the fact that tracer was not mixed uniformly throughout a volume. The fact that timescales for water renewal could be a factor of 2–3 different depending on the method of estimation used means we should be cautious in interpreting the "residence time." Based on results here we may conclude that the *relative* timescales among basins are reasonably well determined by all methods, but the actual values of the timescales require consideration of other factors that may influence a specific tracer, as for example the effects on hypoxia of photosynthesis, air-sea gas exchange, and water column and benthic rates of the remineralization of sinking organic matter.

There are a number of limitations of the box model presented here that should be kept in mind. It is only as accurate as the LiveOcean transports used to create it, and these are hard to validate directly because of the relative lack of current meter data. There is uncertainty in the estimation of reflux coefficients, and in the translation of those to the box model. The box model assumes static forcing over a season and so cannot capture events like large pulses of river flow. Finally, the number of segments chosen can influence the results. For example, the flushing times are essentially like the no-reflux residence times in the limit of a single box instead of many segments and two layers, and the results in Figure 12 and Table 1 clearly show that adding more boxes increases residence time by resolving regions with slower flushing. It is an open question whether or not adding more segments would significantly increase the residence time further. Pursuing this line of reasoning leads to the conclusion that detailed problems are better studied with the full model, whereas the box model excels as a very fast tool for initial estimation and understanding.

While this paper focuses largely on the economically and ecologically important Salish Sea, the methods and results are applicable across all estuaries. The combined use of TEF with efflux/reflux is a valuable

approach likely to prove fruitful in other systems. Moreover, the importance of considering efflux/reflux and incomplete tracer homogenization are expected to be critical to understanding residence times in many estuaries.

Data Availability Statement

All code used in the analysis is archived and available at 10.5281/zenodo.4282775, in particular in the x_tef folder. Model input parameters are in the folder forcing/dot_in/cas6_v3_lo8b. The TEF section extractions and processed files required to run the box model are archived and freely available here (start with the README.txt in the folder after extraction):https://pm2.blob.core.windows.net/pm-share/LO_TEF_data_2020_11.tar.gz.

Acknowledgments
This work was supported with funding from the Washington Ocean Acidification Center (P. MacCready, R. McCabe), NSF grants OCE-1634148 and OCE-1736242 (P. MacCready), NOAA Monitoring and Event Response for Harmful Algal Bloom (MERHAB) grant NA16NOS4780189 (P. MacCready, R. McCabe), ongoing support from the IOOS regional association NANOOS (P. MacCready), and by the Joint Institute for the Study of the Atmosphere and Ocean (JISAO) under NOAA Cooperative Agreement NA15OAR4320063 (R. McCabe). This is NOAA MERHAB contribution 230, and JISAO contribution 2020–1117. M. Lorenz was supported by the Training Group Baltic TRANSCOAST GRK 2000 funded by the German Research Foundation. SNG was supported by NSF Postdoctoral Research Fellowship OCE-1226406. The way of expressing the salt budget in Equation 4 is due to W. Rockwell Geyer. Thanks to cmocean for colormaps (Thyng et al., 2016). The statements, findings, conclusions, and recommendations are those of the authors and do not reflect the views of NSF, NOAA, or the Department of Commerce. The authors are not aware of any real or perceived financial conflicts of interests for any author, nor of other affiliations for any author that may be perceived as having a conflict of interest with respect to the results of this paper.

References

Banas, N. S., Conway-Cranos, L., Sutherland, D. A., MacCready, P., Kiffney, P., & Plummer, M. (2014). Patterns of river influence and connectivity among subbasins of puget sound, with application to bacterial and nutrient loading. *Estuaries and Coasts*, *38*(3), 735–753. https://doi.org/10.1007/s12237-014-9853-y

Bretschneider, D. E., Cannon, G. A., Holbrook, J. R., & Pashinski, D. J. (1985). Variability of subtidal current structure in a fjord estuary: Puget sound, Washington. *Journal of Geophysical Research*, *90*(11), 11949–11958. https://doi.org/10.1029/JC090iC06p11949

Burchard, H., Bolding, K., Feistel, R., Gräwe, U., Klingbeil, K., MacCready, P., et al. (2018). The Knudsen theorem and the Total Exchange Flow analysis framework applied to the Baltic Sea. *Progress in Oceanography*, *165*, 268–286. https://doi.org/10.1016/j.pocean.2018.04.004

Chen, S.-N., Geyer, W. R., Ralston, D. K., & Lerczak, J. A. (2012). Estuarine exchange flow quantified with isohaline coordinates: Contrasting long and short estuaries. *Journal of Physical Oceanography*, *42*(5), 748–763. https://doi.org/10.1175/jpo-d-11-086.1

Cokelet, E. D., & Stewart, R. J. (1985). The exchange of water in fjords: The efflux/reflux theory of advective reaches separated by mixing zones. *Journal of Geophysical Research*, *90*(C4), 7287–7306. https://doi.org/10.1029/JC090iC04p07287

Cokelet, E. D., Stewart, R. J., & Ebbesmeyer, C. C. (1991). *Concentrations and ages of conservative pollutants in Puget Sound*. Paper presented at the Puget Sound Research '91. Puget Sound Water Quality Authority.

Collias, E., McGary, N., & Barnes, C. A. (1974). *Atlas of physical and chemical properties of Puget Sound and its surrounding approaches*, Seattle: University of Washington, Department of Oceanography.

Conroy, T., Sutherland, D. A., & Ralston, D. K. (2020). Estuarine exchange flow variability in a seasonal, segmented estuary. *Journal of Physical Oceanography*, *50*(3), 595–613. https://doi.org/10.1175/jpo-d-19-0108.1

Crean, P. B., & Ages, A. B. (1971). *Oceanographic records from twelve cruises in the Strait of Georgia and Juan de Fuca strait, 1968*, Canada: Department of Energy, Mines and Resources.

Delhez, É. J. M., Heemink, A. W., & Deleersnijder, É. (2004). Residence time in a semi-enclosed domain from the solution of an adjoint problem. *Estuarine, Coastal and Shelf Science*, *61*(4), 691–702. https://doi.org/10.1016/j.ecss.2004.07.013

Deppe, R. W., Thomson, J., Polagye, B., & Krembs, C. (2018). Predicting deep water intrusions to Puget sound, WA (USA), and the seasonal modulation of dissolved oxygen. *Estuaries and Coasts*, *41*, 114–127. https://doi.org/10.1007/s12237-017-0274-6

Ebbesmeyer, C. C., & Barnes, C. A. (1980). Control of a fjord basin's dynamics by tidal mixing in embracing sill zones. *Estuarine and Coastal Marine Science*, *11*, 311–330. https://doi.org/10.1016/S0302-3524(80)80086-7

Ebbesmeyer, C. C., Word, J. Q., & Barnes, C. A. (1988). *Puget sound: A Fjord system homogenized with water recycled over sills by tidal mixing*. In Hydrodynamics of estuaries (Vol. II, pp. 17–29).

Geyer, W. R., & Cannon, G. A. (1982). Sill processes related to deep water renewal in a fjord. *Journal of Geophysical Research*, *87*, 7985. https://doi.org/10.1029/JC087iC10p07985

Geyer, W. R., & MacCready, P. (2014). The Estuarine circulation. *Annual Review of Fluid Mechanics*, *46*, 175–197. https://doi.org/10.1146/annurev-fluid-010313-141302

Gregg, M. C., & Pratt, L. J. (2010). Flow and hydraulics near the sill of Hood Canal, a strongly sheared, continuously stratified Fjord. *Journal of Physical Oceanography*, *40*, 1087–1105. https://doi.org/10.1175/2010JPO4312.1

Hagy, J. D., Boynton, W. R., & Sanford, L. P. (2000). Estimation of net physical transport and hydraulic residence times for a coastal plain estuary using box models. *Estuaries*, *23*, 328–340. https://doi.org/10.2307/1353325

Hansen, D. V., & Rattray, M., Jr. (1965). Gravitational circulation in straits and estuaries. *Journal of Marine Research*, *23*, 104–122.

Khangaonkar, T., Yang, Z., Kim, T., & Roberts, M. (2011). Tidally averaged circulation in Puget Sound sub-basins: Comparison of historical data, analytical model, and numerical model. *Estuarine, Coastal and Shelf Science*, *93*, 305–319. https://doi.org/10.1016/j.ecss.2011.04.016

Knudsen, M. (1900). Ein hydrographischer Lehrsatz. *Annalen der Hydrographie und Maritimen Meteorologie*, *28*, 316–320.

LeBlond, P. H. (1983). The Strait of Georgia: functional anatomy of a coastal sea. *Canadian Journal of Fisheries and Aquatic Sciences*, *40*, 1033–1063. https://doi.org/10.1139/f83-128

Lemagie, E. P., & Lerczak, J. A. (2015). A Comparison of bulk estuarine turnover timescales to particle tracking timescales using a model of the Yaquina Bay estuary. *Estuaries and Coasts*, *38*, 1797–1814. https://doi.org/10.1007/s12237-014-9915-1

Li, M., Gargett, A., & Denman, K. (1999). Seasonal and internannual variability of estuarine circulation in a box model of the Strait of Georgia and Juan de Fuca strait. *Atmosphere: Ocean*, *37*, 1–19. https://doi.org/10.1080/07055900.1999.9649619

Lorenz, M., Klingbeil, K., & Burchard, H. (2020). Numerical Study of the exchange flow of the Persian Gulf using an extended total exchange flow analysis framework. *Journal of Geophysical Research: Oceans*, *125*(2), e2019JC015527. https://doi.org/10.1029/2019jc015527

Lorenz, M., Klingbeil, K., MacCready, P., & Burchard, H. (2019). Numerical issues of the Total Exchange Flow (TEF) analysis framework for quantifying estuarine circulation. *Ocean Science Discussions*, *15*(3), 601–614. https://doi.org/10.5194/os-2018-147

MacCready, P. (2011). Calculating estuarine exchange flow using isohaline coordinates. *Journal of Physical Oceanography*, *41*, 1116–1124. https://doi.org/10.1175/2011JPO4517.1

MacCready, P., & Geyer, W. R. (2010). Advances in estuarine physics. *Annual Review of Marine Science*, *2*, 35–58. https://doi.org/10.1146/annurev-marine-120308-081015

MacCready, P., Geyer, W. R., & Burchard, H. (2018). Estuarine exchange flow is related to mixing through the salinity variance budget. *Journal of Physical Oceanography*, *48*, 1375–1384. https://doi.org/10.1175/JPO-D-17-0266.1

Masson, D., & Peña, A. (2009). Chlorophyll distribution in a temperate estuary: The Strait of Georgia and Juan de Fuca Strait. *Estuarine, Coastal and Shelf Science*, *82*(1), 19–28. https://doi.org/10.1016/j.ecss.2008.12.022

Mofjeld, H. O., & Larsen, L. H. (1984). *Tides and tidal currents of the inland waters of Western Washington*, NOAA Technical Memorandum ERL PMEL-56. Seattle, WA: Pacific Marine Environmental Laboratory. Retrieved from https://www.pmel.noaa.gov/pubs/PDF/mofj687/mofj687.pdf

Monsen, N. E., Cloern, J. E., Lucas, L. V., & Monismith, S. G. (2002). A comment on the use of flushing time, residence time, and age as transport time scales. *Limnology & Oceanography*, *47*(5), 1545–1553. https://doi.org/10.4319/lo.2002.47.5.1545

Moore, S. K., Johnstone, J. A., Banas, N. S., & Salathe, E. P., Jr. (2015). Present-day and future climate pathways affecting Alexandrium blooms in Puget Sound, WA, USA. *Harmful Algae*, *48*, 1–11. https://doi.org/10.1016/j.hal.2015.06.008

Olson, E. M., Allen, S. E., Do, V., Dunphy, M., & Ianson, D. (2020). Assessment of nutrient supply by a Tidal Jet in the northern strait of eorgia based on a biogeochemical model. *Journal of Geophysical Research: Oceans*, *125*(8), e2019JC015766. https://doi.org/10.1029/2019jc015766

Pawlowicz, R. (2001). A tracer method for determining transport in two-layer systems, applied to the Strait of Georgia/Haro Strait/Juan de Fuca Strait Estuarine System. *Estuarine, Coastal and Shelf Science*, *52*(4), 491–503. https://doi.org/10.1006/ecss.2000.0748

Pawlowicz, R., Riche, O., & Halverson, M. (2007). The circulation and residence time of the strait of Georgia using a simple mixing-box approach. *Atmosphere: Ocean*, *45*, 173–193. https://doi.org/10.3137/ao.450401

Peña, M. A., Masson, D., & Callendar, W. (2016). Annual plankton dynamics in a coupled physical–biological model of the Strait of Georgia, British Columbia. *Progress in Oceanography*, *146*, 58–74. https://doi.org/10.1016/j.pocean.2016.06.002

Pinardi, N., Cessi, P., Borile, F., & Wolfe, C. L. P. (2019). The Mediterranean Sea overturning circulation. *Journal of Physical Oceanography*, *49*, 1699–1721. https://doi.org/10.1175/JPO-D-18-0254.1

Ralston, D. K., Geyer, W. R., & Lerczak, J. A. (2008). Subtidal salinity and velocity in the Hudson River Estuary: Observations and modeling. *Journal of Physical Oceanography*, *38*, 753–770. https://doi.org/10.1175/2007JPO3808.1

Rayson, M. D., Gross, E. S., Hetland, R. D., & Fringer, O. B. (2016). Time scales in Galveston Bay: An unsteady estuary. *Journal of Geophysical Research: Oceans*, *121*, 2268–2285. https://doi.org/10.1002/2015JC011181

Rayson, M. D., Gross, E. S., Hetland, R. D., & Fringer, O. B. (2017). Using an isohaline flux analysis to predict the salt content in an unsteady estuary. *Journal of Physical Oceanography*, *47*, 2811–2828. https://doi.org/10.1175/JPO-D-16-0134.1

Riche, O., Johannessen, S. C., & Macdonald, R. W. (2014). Why timing matters in a coastal sea: Trends, variability and tipping points in the Strait of Georgia, Canada. *Journal of Marine Systems*, *131*, 36–53. https://doi.org/10.1016/j.jmarsys.2013.11.003

Seim, H. E., Gregg, M. C. (1994). Detailed observations of a naturally occurring shear instability. *Journal of Geophysical Research*, *99*, 10049–10073. https://doi.org/10.1029/94JC00168

Soontiens, N., Allen, S. E., Latornell, D., Le Souëf, K., Machuca, I., Paquin, J.-P., et al. (2015). Storm Surges in the Strait of Georgia Simulated with a Regional Model. *Atmosphere: Ocean*, *54*(1), 1–21. https://doi.org/10.1080/07055900.2015.1108899

Thomson, R. E., Mihály, S. F., & Kulikov, E. A. (2007). Estuarine versus transient flow regimes in Juan de Fuca Strait. *Journal of Geophysical Research: Oceans*, *112*, 1–25. https://doi.org/10.1029/2006JC003925

Thyng, K. M., Hetland, R. D., Zimmerle, H. M., & DiMarco, S. F. (2016). True colors of oceanography: Guidelines for effective and accurate colormap selection. *Oceanography*, *29*(3), 9–13. https://doi.org/10.5670/oceanog.2016.66

Reference From the Supporting Information

Babson, A. L., Kawase, M., & MacCready, P. (2006). Seasonal and interannual variability in the circulation of Puget Sound, Washington: A box model study. *Atmosphere: Ocean*, *44*, 29–45. https://doi.org/10.3137/ao.440103

Brasseale, E., Grason, E. W., McDonald, P. S., Adams, J., & MacCready, P. (2019). Larval transport modeling support for identifying population sources of European green crab in the Salish Sea. *Estuaries and Coasts*, *42*, 1586–1599. https://doi.org/10.1007/s12237-019-00586-2

Codiga, D. L. (2011). *Unified tidal analysis and prediction using the UTide Matlab functions* (Technical Report 2011-01). Narragansett, RI: University of Rhode Island. Retrieved from http://ftp//www.po.gso.uri.edu/pub/downloads/codiga/pubs/2011Codiga-UTide-Report.pdf

Davis, K. A., Banas, N. S., Giddings, S. N., Siedlecki, S. A., MacCready, P., Lessard, E. J., et al. (2014). Estuary-enhanced upwelling of marine nutrients fuels coastal productivity in the U.S. Pacific Northwest. *Journal of Geophysical Research: Oceans*, *119*(12), 8778–8799. https://doi.org/10.1002/2014jc010248

Egbert, G. D., & Erofeeva, S. Y. (2002). Efficient inverse modeling of barotropic ocean tides. *Journal of Atmospheric and Oceanic Technology*, *19*, 183–204. https://doi.org/10.1175/1520-0426(2002)019<0183:EIMOBO>2.0.CO;2

Emery, W. J., & Thomson, R. E. (1998). *Data analysis methods in physical oceanography*. Oxford: Kidlington Elsevier Science.

Feely, R. A., Alin, S. R., Carter, B., Bednaršek, N., Hales, B., Chan, F., et al. (2016). Chemical and biological impacts of ocean acidification along the west coast of North America. *Estuarine, Coastal and Shelf Science*, *183*, 260–270. https://doi.org/10.1016/j.ecss.2016.08.043

Finlayson, D. P. (2005). *Combined bathymetry and topography of the Puget lowland*. Washington, DC: University of Washington School of Oceanography. Retrieved from https://www.ocean.washington.edu/data/pugetsound/psdem2005.html

Foreman, M. G. G., Walters, R. A., Henry, R. F., Keller, C. P., & Dolling, A. G. (1995). A tidal model for eastern Juan de Fuca Strait and the southern Strait of Georgia. *Journal of Geophysical Research*, *100*, 721–740. https://doi.org/10.1029/94JC02721

Fredrickson, E. K., Wilcock, W. S. D., Schmidt, D. A., MacCready, P., Roland, E., Kurapov, A. L., et al. (2019). Optimizing sensor configurations for the detection of slow-slip earthquakes in seafloor pressure records, using the Cascadia subduction zone as a case study. *Journal of Geophysical Research: Solid Earth*, *124*, 13504–13531. https://doi.org/10.1029/2019JB018053

Giddings, S. N., & MacCready, P. (2017). Reverse estuarine circulation due to local and remote wind forcing, enhanced by the presence of along-coast estuaries. *Journal of Geophysical Research: Oceans*, *122*, 10184–10205. https://doi.org/10.1002/2016JC012479

Giddings, S. N., MacCready, P., Hickey, B. M., Banas, N. S., Davis, K. A., Siedlecki, S. A., et al. (2014). Hindcasts of potential harmful algal bloom transport pathways on the Pacific Northwest coast. *Journal of Geophysical Research: Oceans*, *119*, 2439–2461. https://doi.org/10.1002/2013JC009622

Haidvogel, D. B., Arango, H. G., Hedstrom, K., Beckmann, A., Malanotte-Rizzoli, P., & Shchepetkin, A. F. (2000). Model evaluation experiments in the North Atlantic Basin: Simulations in nonlinear terrain-following coordinates. *Dynamics of Atmospheres and Oceans*, *32*, 239–281. https://doi.org/10.1016/S0377-0265(00)00049-X

Khangaonkar, T., Long, W., & Xu, W. (2017). Assessment of circulation and inter-basin transport in the Salish Sea including Johnstone Strait and Discovery Islands pathways. *Ocean Modelling*, *109*, 11–32. https://doi.org/10.1016/j.ocemod.2016.11.004

Lavelle, J. W., Mofjeld, H. O., Lempriere-Doggett, E., Cannon, G. A., Pashinski, D. J., Cokelet, E. D., et al. (1988). *A multiply-connected channel model of tides and tidal currents in Puget Sound, Washington and a comparison with updated observations*. NOAA technical memorandum ERL PMEL-84. Retrieved from https://www.pmel.noaa.gov/pubs/PDF/lave967/lave967.pdf

Liu, Y., MacCready, P., Hickey, B. M., Dever, E. P., Kosro, P. M., & Banas, N. S. (2009). Evaluation of a coastal ocean circulation model for the Columbia River plume in summer 2004. *Journal of Geophysical Research*, *114*(C2), 1–23. https://doi.org/10.1029/2008jc004929

Mass, C. F., Albright, M., Ovens, D., Steed, R., MacIver, M., Grimit, E., et al. (2003). Regional environmental prediction over the Pacific Northwest. *Bulletin of the American Meteorological Society*, *84*, 1353–1366. https://doi.org/10.1175/BAMS-84-10-1353

Metzger, E. J., Smedstad, O. M., Thoppil, P., Hurlburt, H., Cummings, J., Walcraft, A., et al. (2014). US Navy operational global ocean and Arctic Ice prediction systems. *Oceanography*, *27*(3), 32–43. https://doi.org/10.5670/oceanog.2014.66

Mohamedali, T., Roberts, M., Sackmann, B., Whiley, A., & Kolosseus, A. (2011). *South Puget Sound dissolved oxygen study interim nutrient load Summary for 2006-2007* (8778336341).

Shchepetkin, A. F., & McWilliams, J. C. (2005). The regional oceanic modeling system (ROMS): a split-explicit, free-surface, topography-following-coordinate oceanic model. *Ocean Modelling*, *9*, 347–404. https://doi.org/10.1016/j.ocemod.2004.08.002

Siedlecki, S. A., Banas, N. S., Davis, K. A., Giddings, S. N., Hickey, B. M., MacCready, P., et al. (2015). Seasonal and interannual oxygen variability on the Washington and Oregon continental shelves. *Journal of Geophysical Research: Oceans*, *120*(2), 608–633. https://doi.org/10.1002/2014jc010254

Sutherland, G., Garrett, C., & Foreman, M. (2005). Tidal resonance in Juan de Fuca strait and the strait of Georgia. *Journal of Physical Oceanography*, *35*(7), 1279–1286. https://doi.org/10.1175/jpo2738.1

Sutherland, D. A., MacCready, P., Banas, N. S., & Smedstad, L. F. (2011). A model study of the Salish Sea estuarine circulation. *Journal of Physical Oceanography*, *41*(6), 1125–1143. https://doi.org/10.1175/2011jpo4540.1

Thomson, R. E., & Huggett, W. S. (1980). M2 Baroclinic tides in Johnstone strait, British Columbia. *Journal of Physical Oceanography*, *10*, 1509–1539. https://doi.org/10.1175/1520-0485(1980)010<1509:MBTIJS>2.0.CO;2

Tozer, B., Sandwell, D. T., Smith, W. H. F., Olson, C., Beale, J. R., & Wessel, P. (2019). Global Bathymetry and Topography at 15 Arc Sec: SRTM15+. *Earth and Space Science*, *6*(10), 1847–1864. https://doi.org/10.1029/2019ea000658

AGU PUBLICATIONS

Journal of Geophysical Research Oceans

Supporting Information for

Estuarine Circulation, Mixing, and Residence Times in the Salish Sea

P. MacCready[1], R. M. McCabe[2,3], S. A. Siedlecki[4], M. Lorenz[5], S. N. Giddings[6], J. Bos[7], S. Albertson[7], N. S. Banas[8], S. Garnier[8]

[1]University of Washington, School of Oceanography.
[2]University of Washington, Joint Institute for the Study of the Atmosphere and Ocean, Seattle, WA, USA.
[3]University of Washington, Cooperative Institute for Climate, Ocean, and Ecosystem Studies, Seattle, WA, USA.
[4]University Connecticut, Department of Marine Sciences.
[5]Leibniz Institute for Baltic Sea Research Warnemünde, Rostock, Germany.
[6]University of California, San Diego.
[7]Washington State Department of Ecology.
[8]University of Strathclyde.
Corresponding author: Parker MacCready (pmacc@uw.edu)

Contents of this file

Text S1 to S3
Figures S1 to S11

Introduction

The supplemental information in S1 consists of a detailed description of the LiveOcean model set-up. In S2 extensive model validation results are given. In S3 some more information on annual-mean tidal energy flux and volume transport throughout the model domain is presented.

Text S1. Model Setup

The realistic numerical model used here is created using the Regional Ocean Modeling System (ROMS) (Haidvogel et al., 2000; Shchepetkin & McWilliams, 2005) which integrates the Reynolds averaged, Boussinesq, incompressible equations of motion and tracer concentration on a rotating, spherical grid. It is widely used for coastal and estuarine studies because its design allows for practical optimization of choices of open boundary conditions, turbulence closure, and advection algorithms. The model configuration here is based on fifteen years of research and modeling in the region, typically tightly linked to large observational studies, as reviewed in Giddings et al. (2014). The specific model configuration used here is called LiveOcean, specifically the version of LiveOcean designated as cas6_v3_lo8b. The model domain covers all of Oregon, Washington, and most Vancouver Island coastal waters, and the Salish Sea – the name for the combined inland waters of Puget Sound, the Strait of Georgia, and the Strait of Juan de Fuca (Fig. S1). The model grid follows lines of constant longitude and latitude, with 500 m spacing in most of the Salish Sea and Washington coastal estuaries, stretching to 1500 m at the north end of Strait of Georgia, and 3000 m on the north, south and west model open boundaries (1320 rows, 663 columns). The model bathymetry is a combination of the Tozer et al. (2019) SRTM15+ product (~500 m), a combined product described in D. A. Sutherland et al. (2011) for the Salish Sea (~400 m), and the Finlayson (2005) Puget Sound bathymetry (~183 m), with smoothing as described in Giddings et al. (2014). The vertical S-coordinates consist of 30 layers spaced between the local bottom and free surface, with closer spacing near the bottom and top. The grid was designed to simulate coastal and estuarine processes accurately enough to capture important interactions such as the influence of the Columbia River on flow reversals in Juan de Fuca (Giddings & MacCready, 2017) or the influence of the Juan de Fuca estuarine outflow on Washington shelf productivity (Davis et al., 2014). The present grid covers a larger domain and has three times finer resolution, required for effective simulation of the Salish Sea and coastal estuaries. The model grid has an enforced minimum depth of 4 m, and does not include wetting-and-drying because the intertidal is poorly resolved at 500 m.

The model is forced with daily averaged flow from 45 rivers (Fig. S2), using gauged flow from USGS and Environment Canada. Many of the Salish Sea rivers are adjusted for ungauged watershed, or use flow estimated from nearby gauged rivers, using scaling factors from Mohamedali et al. (2011). The LiveOcean model is run quasi-operationally to create a three-day forecast every day, and in 14

cases river flow forecasts are available from the NOAA Northwest River Forecast Center; otherwise persistence from the real-time data is assumed to fill out flow in forecast days. River temperature is specified using annual cycles developed based on proximity to the 11 rivers that have historical temperature data available (river names in red on Fig. S2). Tides are forced along the three open boundaries using gridded phase and amplitude values from TPXO 7.2 (Egbert & Erofeeva, 2002) for 8 constituents (M_2, S_2, K_1, O_1, N_2, P_1, K_2, Q_1). Tidal forcing was adjusted to obtain optimal comparison with observations (see Text S2). Constituent amplitudes were multiplied by factors from 1.21 to 1.43; why such a large amplification was required is unknown but it may reflect the missing gravitational tractive force over the domain. Atmospheric forcing comes from the WRF model run by Dr. Cliff Mass at University of Washington (Mass et al., 2003) as a three day forecast. Over most of the model domain the WRF resolution is 1.4 km, with 4.2 km and 12.5 km grids used as needed (Fig. S3). This fine resolution represents a substantial improvement over products previously used to model the Salish Sea, although the impact of the better resolution is not quantified here. The atmospheric forcing provides wind stress and all heat fluxes, as described in (Giddings et al., 2014). Evaporation and precipitation are not included as part of the salinity surface boundary condition. This was tried but had negligible effect on validation results – not surprising given the huge influence of rivers in this region. Open ocean boundary conditions come from the global, data-assimilative, community ocean model HYCOM (Metzger et al., 2014), which has 4.5 km resolution in this region. Daily boundary values of velocity, temperature, salinity and sea surface height are smoothed with a 5-day Hanning window to remove aliased inertial oscillations. Radiative boundary conditions are used in ROMS, as well nudging to the full 3-D field of HYCOM values over a 6-gridpoint region around the open boundary, as detailed in Giddings et al. (2014). HYCOM fields are available online as 10-day forecasts.

The model run analyzed here is a three-year hindcast, initialized on Dec. 15, 2016 with HYCOM values offshore and observed water properties from the WA State Dept. of Ecology and Fisheries and Oceans Canada within the Salish Sea and WA coastal estuaries (Grays Harbor and Willapa Bay). We analyze the period 2017-2019. Model fields accumulate daily, with day one of the ongoing three-day forecast added each day as that day of the hindcast. The forecast workflow consists of a series of Linux cron jobs on several computers. These gather data on rivers, ocean, and atmospheric state from external sources as described above and then create the forcing fields for ROMS. The model is run on a Linux cluster every morning and takes about 2 hours on 196 cores with a baroclinic time step of 40 seconds. Occasionally the model blows up, e.g. due to strong

currents during spring tides. In this case the driver script automatically restarts the run with a smaller time step. Other automated methods of handling occasional missing forcing data are built into the system, ensuring good reliability, although daily human attention is still essential. The daily forecasts are used to give shellfish growers information about aragonite saturation state in WA coastal estuaries. It also has particle tracking in daily post-processing which is used in combination with beach sampling by resource managers who decide when to open WA beaches for razor clam harvest. These beaches are occasionally impacted by harmful algal blooms (HABs) associated with domoic acid produced by marine diatoms of the genus Pseudo-nitzschia. Model fields are also used by other modelers in the region for open boundary conditions. Model fields are available as graphical overlays through NANOOS (http://nvs.nanoos.org/Explorer), the IOOS EDS Viewer (https://eds.ioos.us/), and the LiveOcean website (http://faculty.washington.edu/pmacc/LO/LiveOcean.html).

The motivations and funding for building this model and maintaining forecasts are largely biogeochemical: HABs (Davis et al., 2014; Giddings et al., 2014), hypoxia (Siedlecki et al., 2015), ocean acidification, larval dispersal of invasive species (Brasseale et al., 2019), and pressure signals associated with slow-slip earthquakes (Fredrickson et al., 2019). The model includes tracers representing nitrate, phytoplankton, zooplankton, two sizes of detritus, dissolved oxygen, total inorganic carbon, and alkalinity. The NPZDO formulations use parameter choices described in (Davis et al., 2014) and (Siedlecki et al., 2015). Open boundary values for the biogeochemical variables are specified using regressions against salinity from offshore data collected during NOAA cruises (Feely et al., 2016). The regressions are given in forcing/ocn4/Ofun_bio.py in the code archive: 10.5281/zenodo.4282775.

Text S2. Model Validation

The three-year model hindcast has been extensively compared to observations. A summary of those comparisons is presented here, focusing particularly on elements most relevant to the exchange flow in the Salish Sea.

Tides are a key concern for the exchange flow because it is mainly the conversion of tidal energy to turbulence that forces mixing of fresh and saltwater. We use observed hourly sea surface height (SSH) from 21 tide stations, 13 from NOAA and 8 from Fisheries and Oceans Canada (DFO),

throughout the Salish Sea and coastal ocean. The average root mean square error (RMSE) is 31 cm, about 15% of the typical tide range of 2 m. For comparison, the SSH error reported in Khangaonkar et al. (2017) for a realistic model of this region is 10% of the tidal range, although what tidal range was assumed is not stated. The SSH performance here is a significant improvement over the MoSSea model (D. A. Sutherland et al., 2011), in which the amplitude of semi-diurnal constituents at Seattle was only 75% of observed. Extensive experiments (not shown) found that the improvement reported here occurred only when we extended the grid around Vancouver Island, opening Johnstone Strait and allowing significant tidal energy to leave the Salish Sea by that route. A hypothesis for why this might improve the semi-diurnals in Puget Sound is that the reduced reflection "detunes" the half-wave in the primary Juan de Fuca-Strait of Georgia channel, making tide range higher near the node – and hence at Admiralty Inlet, the seaward boundary for Puget Sound. An example from the tide station at Seattle (Fig. S4) shows hourly comparisons for a month of 2017 (Fig. S4a); the model does a good job of reproducing the mixed semi-diurnal tides here. The error (Fig. S4a, gray line) is mainly due to phase: all tidal constituents ended up with a phase lag of about an hour compared to observations throughout the model, for unknown reasons. While this is a clear target for future model improvements, it should have limited influence on the tidally averaged mixing due to tides. Tidally averaged SSH, created using the Godin 24-24-25 filter (Emery & Thomson, 1998), is plotted in Fig. S4b. Both observed (red) and modeled (blue) curves exhibit a bumpy annual cycle, with SSH lower in summer by about 30 cm due to set-down at the coast caused by upwelling-favorable (northerly) winds at the coast – which force surface Ekman transport offshore. However, the observed signal has significantly more high-frequency bumps than the model. This is apparently due to the "inverted barometer effect" in which lower atmospheric pressure raises SSH, as evidenced by the fact that when we added this effect to the model curve (going from the blue line to the light blue line in Fig. S4b) nearly all of the observed signal was recovered. The inverted barometer effect was not included in the version of the model run here. Harmonic analysis was performed with the UTide package (Codiga, 2011) using the Python version (https://github.com/wesleybowman/UTide). Results are presented for amplitude (Fig. S4c) and phase (Fig. S4d) for the 5 largest constituents. The match is reasonable in all cases, although the model phase lag mentioned above is apparent. Phase and amplitude for all 21 stations are shown for the largest semi-diurnal constituent, M_2 (Fig. S5a), and the largest diurnal constituent, K_1 (Fig. S5b). These clearly exhibit the characteristics described in G. Sutherland et al. (2005) where the semi-diurnal tide has the character of a half-wave with a node near Victoria, BC

and near-180° phase shift from the coast to the inland waters. The diurnal tide is more of a quarter-wave oscillator, with notable amplification in the inland waters compared to the coast.

Water properties are compared with observations at 39 stations with approximately monthly data from the WA Dept. of Ecology and Environment Canada; of these 8 out of 39 were in the coastal estuaries Willapa Bay and Grays Harbor. Comparisons are presented for 2017, the year with the most complete observational record. Error statistics were similar for the other years. Comparisons were made at 3 or 4 nominal depths: 0, 10, 30 and 80 m, the first three corresponding to the nominal depths for bottle samples from WA Dept. of Ecology, e.g. for nitrate. An example annual time series for a station in Whidbey Basin is shown in Fig. S6, showing that the model has good skill at capturing the temporal and depth variation of salinity and temperature. As is typical of variables affected by biological processes, the model skill with dissolved oxygen (DO) and dissolved inorganic nitrogen (DIN) is reasonable but not as good as that for the physical variables. DIN in the observations is the sum of nitrate, nitrite and ammonium, while in the model it is only nitrate because the model does not have other explicit DIN components and so implicitly combines all three into one form. Summary scatterplots and statistics for all stations and 4 depths are shown in Fig. S7. The choice to use only 4 depths is important: it implies we consider the top ~20 m to be of equal importance to everything below, consistent with the skill-averaging strategy in Liu et al. (2009). Salinity (Fig. S7a) has most error at the surface and is biased slightly high, possibly due to the lack of precipitation in the forcing, while temperature (Fig. S7b) is biased slightly low. DO in the model shows reasonable skill (Fig. S7c) with some tendency to be too high near the surface and too low at depth. DIN has considerably more scatter (Fig. S7d), but the high and low endpoints are reasonable. A different approach would be to calculate error statistics using 1 m data from the full range of depths; however, this implies that the vast bulk of water below the 10-20 m pycnocline has much more importance than the surface water. If we take this approach the error statistics are about improved, with salinity RMSE (bias) = 0.97 (0.58) g kg^{-1}, temperature RMSE (bias) = 0.73 (-0.52) °C, and dissolved oxygen RMSE (bias) = 1.09 (-0.35) mg L^{-1}. These numbers are from combining all 3 years, 2017-9. Despite a significant temporal increase of salinity in the Salish Sea: 0.68 g kg^{-1} over three years estimated from the CTD data, the salinity bias for stations inside Puget Sound stayed roughly the same in each year (0.62, 0.60, 0.53) implying that the modeled salinity drift was capturing a real trend, and not a spurious model artifact.

Taken as a whole, these comparisons suggest that the model fields are reasonably similar to the observations, and that we may therefore use the model to explore the estuarine exchange flow. While the bulk of the analysis in the paper is focused on volume and salt transports, the validation results for temperature, dissolved oxygen, and nitrate presented here give independent lines of evidence that the model circulation is realistic. This conclusion is supported by a moored record of currents in Haro Strait collected by NOAA as part of a larger effort to update the tides and currents predictions for the region. Haro Strait is the main connection between the Strait of Georgia and the Strait of Juan de Fuca (Fig. S1b). The modeled subtidal flow there, Fig. S8, compares reasonably well with observations, in particular for the along channel velocity where a clear estuarine exchange flow is evident.

Turning to the coast, the model was evaluated at many mooring locations on the shelf and slope. Time series from one location on the Washington shelf are shown in Fig. S9, for temperature, salinity and DO. In general the model has good skill on the shelf, and performs at least as well as previous versions (Davis et al., 2014; Giddings et al., 2014; Siedlecki et al., 2015), and likely benefits from the finer grid, additional rivers, and finer scale wind forcing. Water property summary statistics for 14 mooring record comparisons on the shelf are shown in Fig. S10. Data for these comparisons come from the Olympic Coast National Marine Sanctuary, NANOOS, and the NSF Ocean Observatories Initiative Endurance Array.

Text S3. Mean transports

Using the TEF extractions we can calculate the annual average tidal energy flux and net volume transport through each section. Results for these are presented in Fig. S11. The tidal energy flux (Fig. S11a,b) shows patterns consistent with previous model-data analyses for Juan de Fuca-Strait of Georgia (Foreman et al., 1995) and Puget Sound (Lavelle et al., 1988). The tidal energy flux is calculated considering only barotropic pressure work. About 6 GW of tidal energy flux enters the Strait of Juan de Fuca and about a third of that gets into Strait of Georgia – with significant loss of 1.5 GW in the intense flows through the narrow channels around the San Juan Islands at the south end of Strait of Georgia. Notably, of the 2 GW that gets into the Strait of Georgia, almost half escapes through Johnstone Strait at the northern end, suggesting that the Strait of Georgia is significantly less reflective than assumed by previous authors such as G. Sutherland et al. (2005). In Puget Sound there is an influx of 631 MW (estimated as 733 MW in Lavelle et al. (1988)), with

significant losses as expected in Admiralty Inlet and Tacoma Narrows. Strikingly, there is little net energy flux, less than 0.5 MW, through most of the Hood Canal sections, suggesting that little of the energy of tidal motion is dissipated there. This is consistent with the many previous characterizations of Hood Canal as a relatively stagnant branch of Puget Sound with long residence times (Babson et al., 2006).

The pattern of net volume flux (Fig. S11c,d) is controlled by annual mean river flows and is only subject to uncertainty in multiply connected basins where the complete model dynamics determines net flow. For example, the model predicts an average of about 3779 $m^3 s^{-1}$ entering the northern Strait of Georgia. This is significant because it is about half of the net of all rivers entering the Salish Sea, although of course it is mostly seawater, not freshwater. It is also in the opposite direction to the ~1000 $m^3 s^{-1}$ net transport reported leaving the northern Strait of Georgia reported from a similarly comprehensive model in Khangaonkar et al. (2017). Observationally this transport was estimated to be around 0±1000 $m^3 s^{-1}$ (Thomson & Huggett, 1980). All are small compared to the estimated magnitude of the estuarine exchange flow there, which is about 25,000 $m^3 s^{-1}$ in the present model. A surprise in the net transport (Fig. S11d) is that most of the net flow out of Puget Sound is through Deception Pass (the 1257 $m^3 s^{-1}$ flux near the top of that panel) and much less goes out through the larger Admiralty Inlet, although the exchange flow is completely dominated by Admiralty Inlet. Nearly the same pattern for Deception Pass is seen in the model results of Khangaonkar et al. (2017), presenting a challenge for observations.

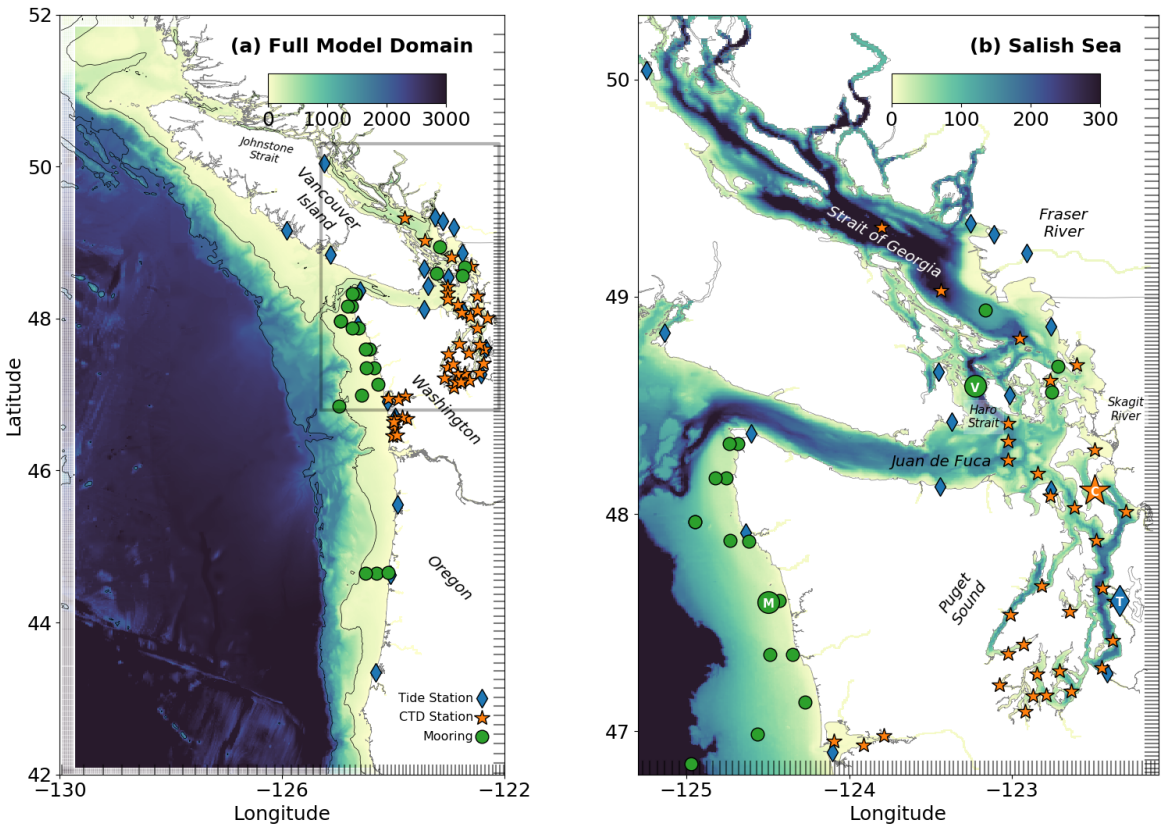

Figure S1. *LiveOcean model domain (a) colored by depth [m]. Grid spacing is indicated with tick marks (only every 10th grid point is drawn). Region of nudging to climatology at open boundaries is indicated by transparency. Close up of the model (b) for the Salish Sea with ticks for every 4th grid point. Station locations for tides, CTD casts, and moorings used in validation are indicated with symbols. Larger station symbols with letters (T, C, M, V) in (b) denote places where time series are shown in subsequent plots.*

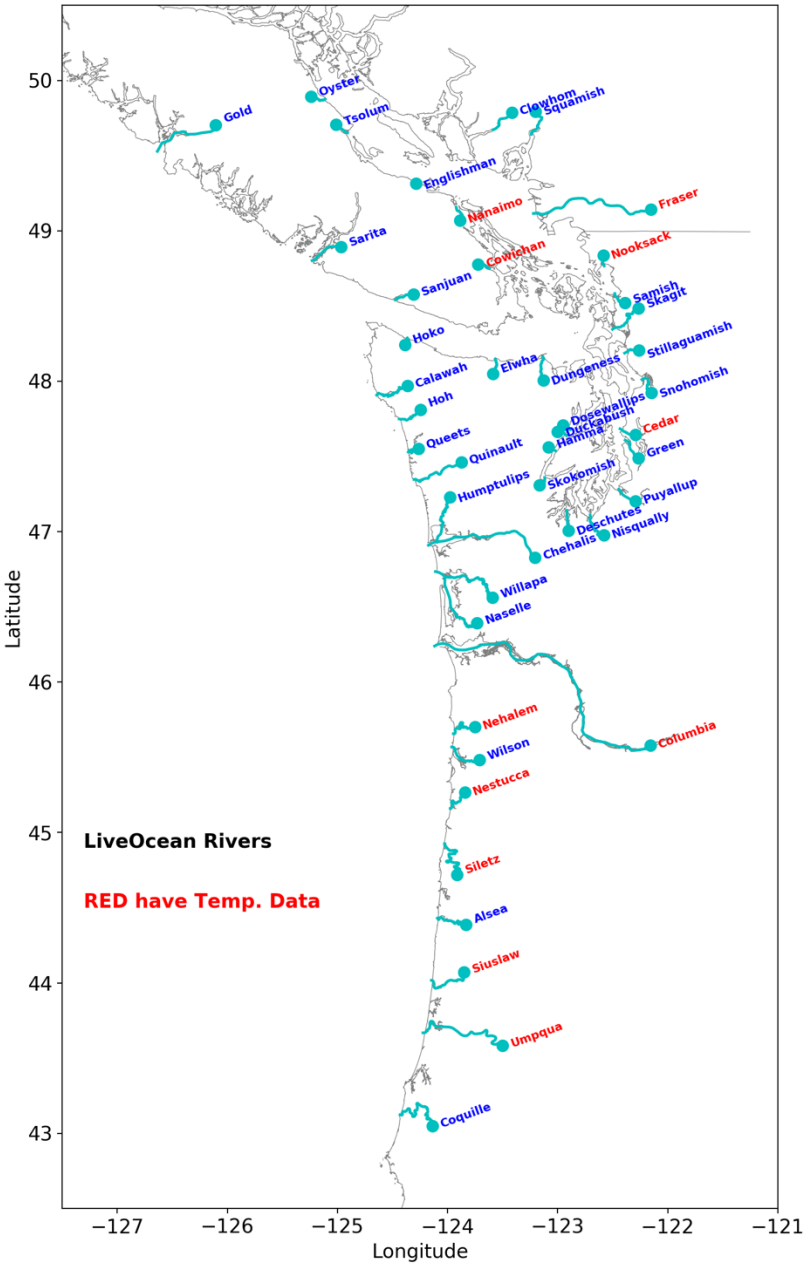

Figure S2. *Names and locations of the 45 rivers used in the LiveOcean model. Rivers with names in red text have historical temperature data available that was sufficient to construct the annual temperature climatology used for forcing. The cyan lines indicate carved river channels determined by USGS data when available and hand-digitized through GIS/Google Earth. Cyan dots indicate the river discharge points in the model.*

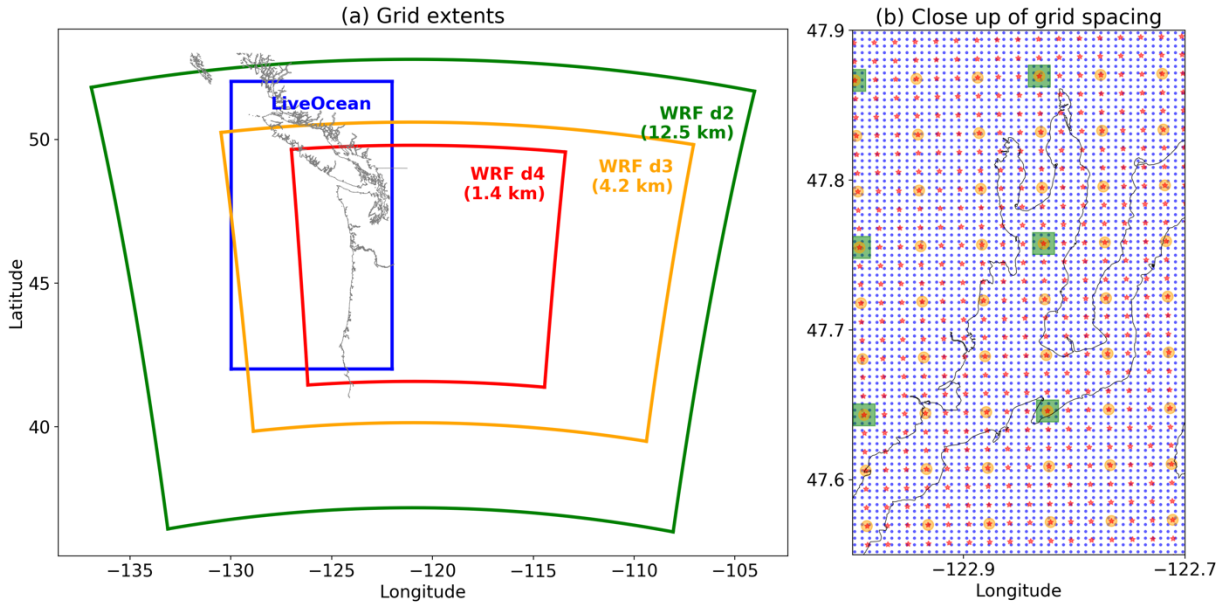

Figure S3. *Grid extents for the three WRF models used for atmospheric forcing are plotted in (a), along with their grid resolution and the extent of the LiveOcean grid (blue). Grid spacing for the three WRF models and for LiveOcean are shown (b) for a small portion of the grid on Hood Canal, with colors matching the outlines in (a).*

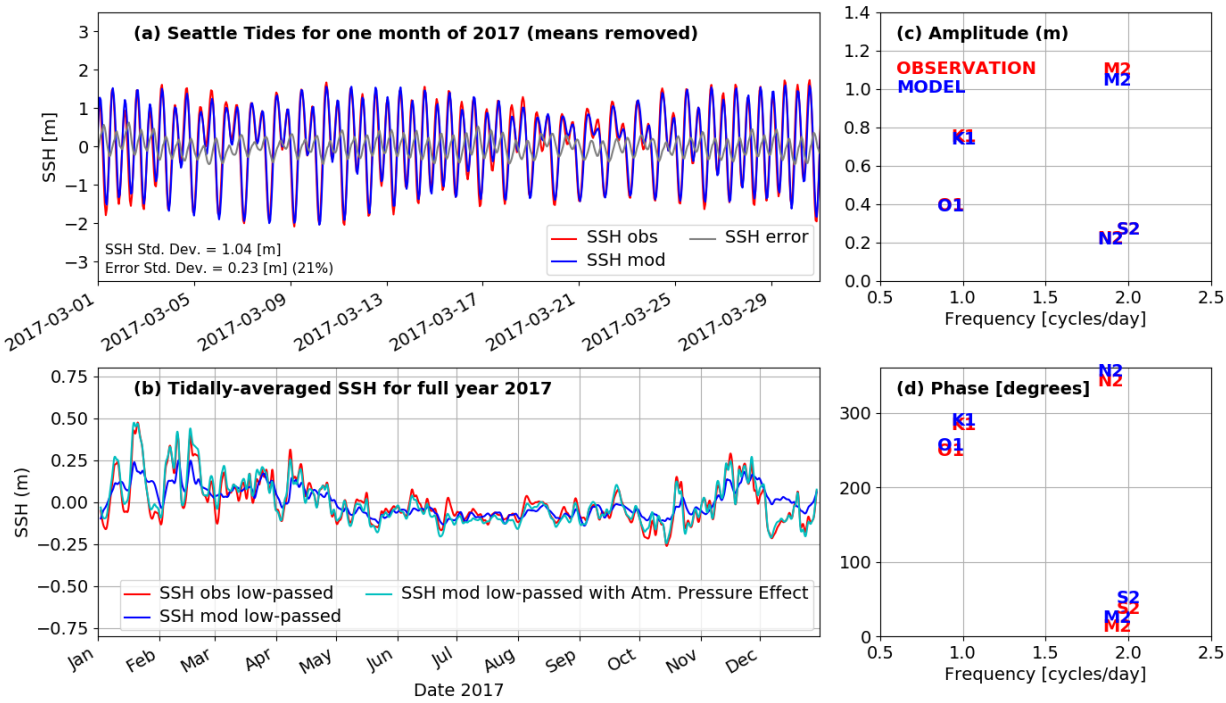

Figure S4*. Comparison of observed (red) and modeled (blue) sea surface height (SSH) at the Seattle tide station for 2017 (tide station "T" in Fig S1b). Hourly values for one month are shown in (a). Low-passed SSH for the whole year is plotted in (b). The light blue line in (b) is the model low-passed SSH adjusted to include the "inverse barometer effect" using atmospheric pressure. The results of harmonic analysis of the full year are shown for the 5 most important constituents as amplitude (c) and phase (d).*

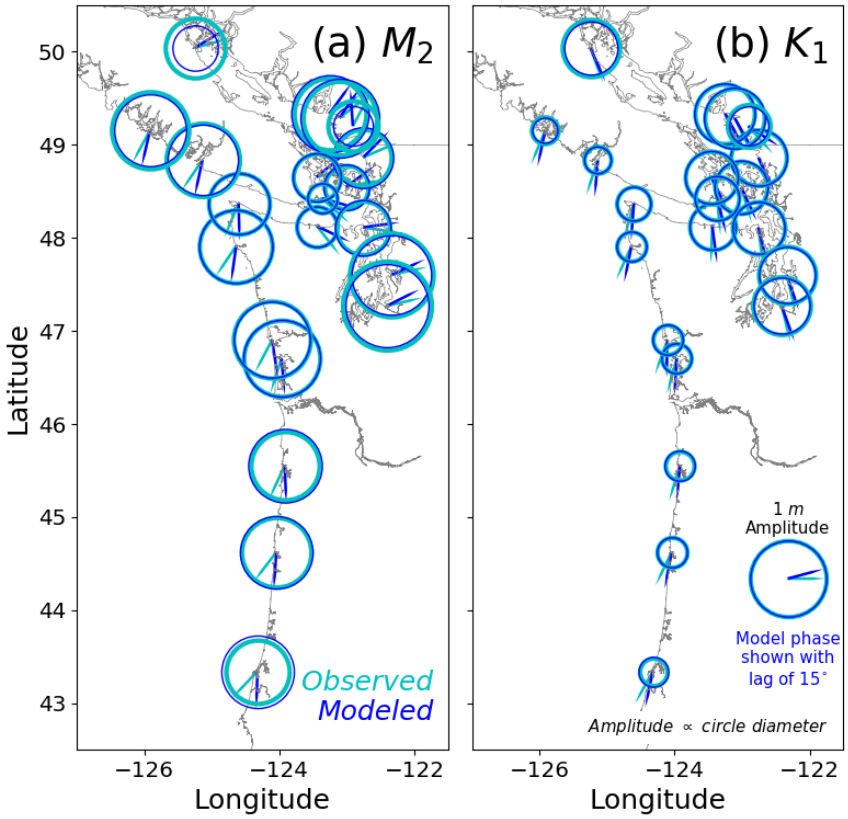

Figure S5*. Comparison of observed (light blue) and modeled (dark blue) tidal phase and amplitude for 2017 at 21 tide stations. Amplitude is shown as circle diameter and phase by pointers inside each circle: 360° of phase is one period for the given constituent, and phase increases counterclockwise. The primary semidiurnal constituent, M_2 (12.42 hour period), is plotted in (a), and the primary diurnal constituent, K_1 (23.93 hour period), in (b). The amplitudes match well throughout. The model phase lags the observed by about an hour, however the spatial patterns are consistent with observations.*

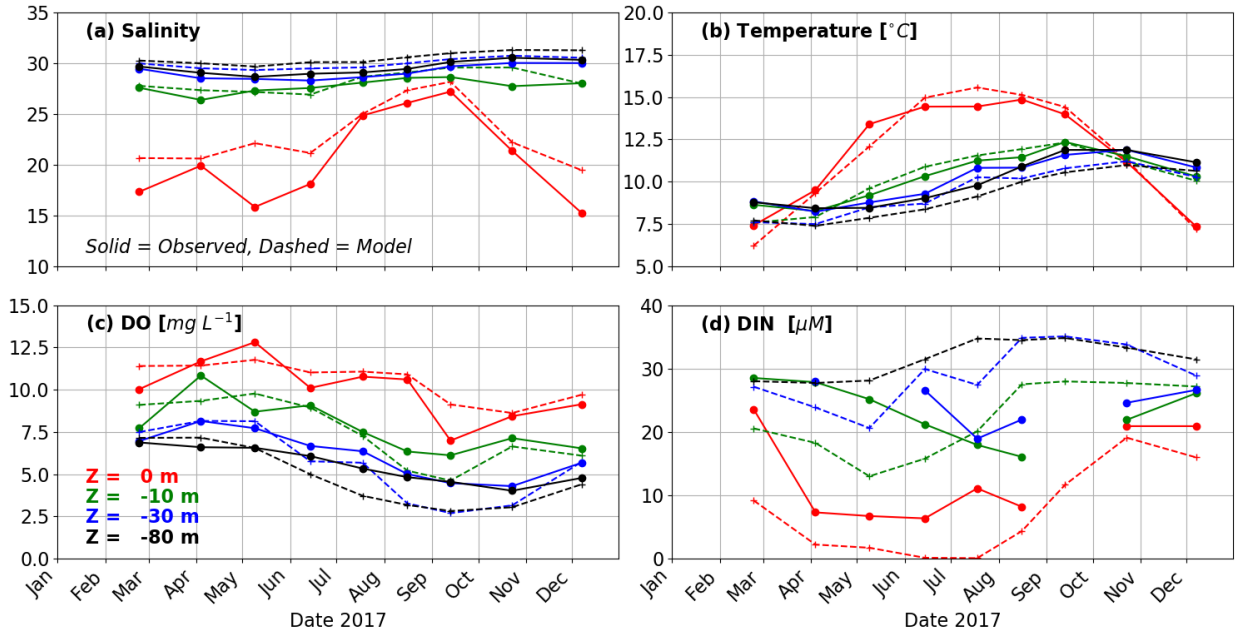

Figure S6. *Time series for 2017 of monthly water properties from a station occupied by the WA Dept. of Ecology in Whidbey Basin (CTD station "C" in Fig. S1b). Each time series is shown at four depths and compares observed (solid line) and modeled (dashed line) values. Salinity (a) reflects the fresh surface water from the Skagit River. Temperature (b) shows a typical annual cycle due to surface heating. Dissolved oxygen, DO, (c) is lower at depth, while dissolved inorganic nitrogen, DIN, (d) is higher at depth. DIN drops to low values at the surface during the Spring. Overall the model-data comparisons show increasing error for fields like DO and DIN which involve biology.*

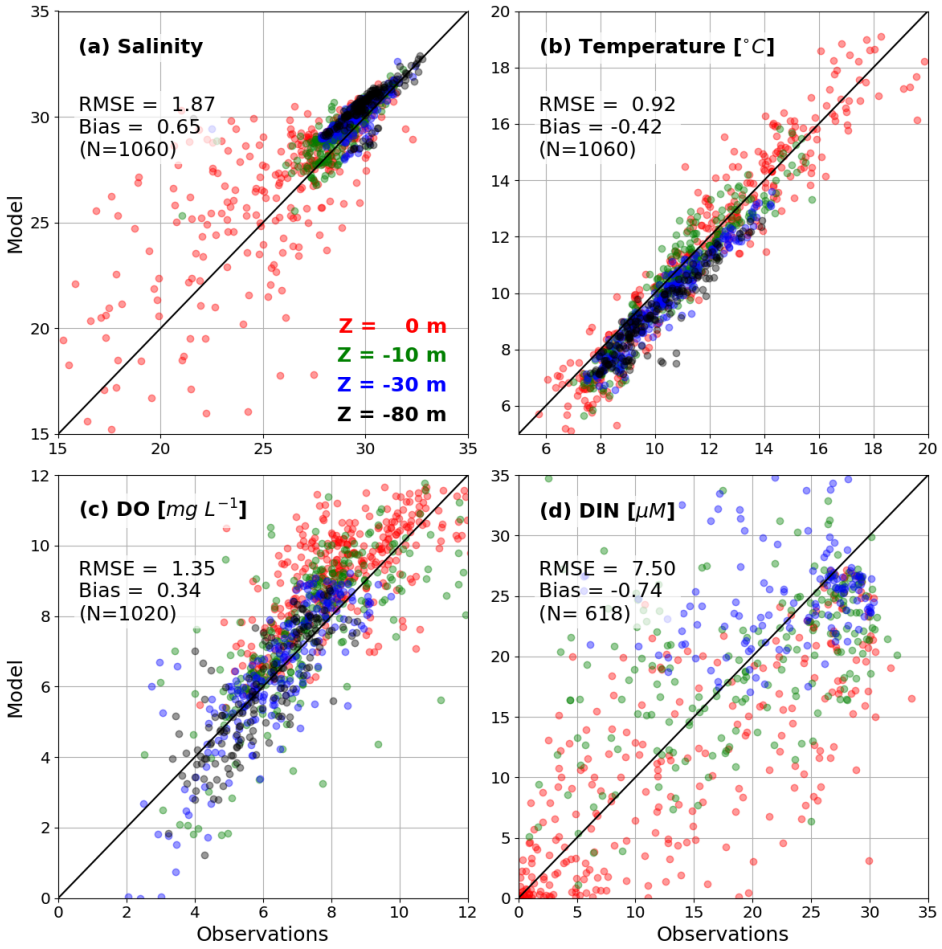

Figure S7*. Scatterplots comparing observed and modeled properties from CTD casts and bottles at 39 stations occupied approximately monthly during 2017. Properties are plotted at 4 depths, with statistical comparisons (RMSE and Mean Bias) and number of samples (N) in each plot. Lines indicating a perfect 1:1 correlation are shown.*

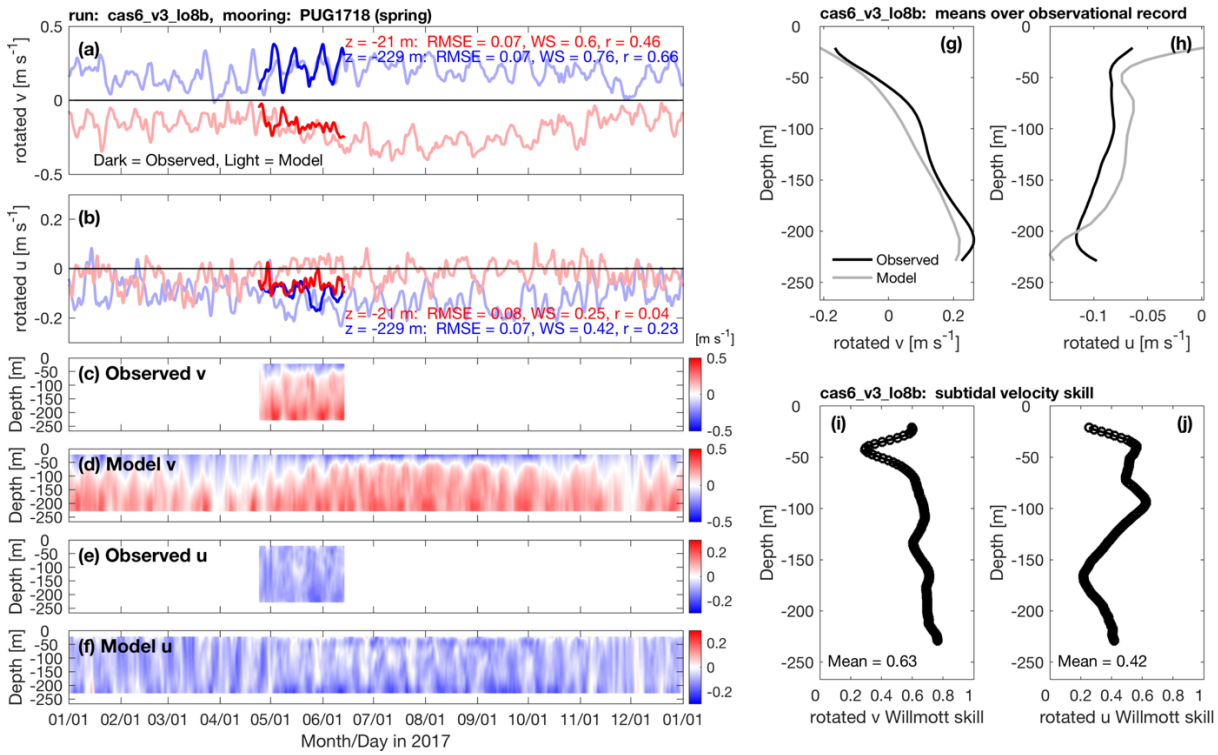

Figure S8. *Comparison of observed and modeled tidally averaged currents from a NOAA mooring in Haro Strait (mooring station "V" in Fig. S1b) the main channel connecting the Strait of Juan de Fuca and Strait of Georgia. Along channel (a) and cross channel (b) currents at two depths are plotted with dark lines for the observations and transparent lines for the model. Full-depth plots of the same fields are shown in (c-f), with observation-record means vs. depth in (g) and (h). Willmott skill vs. depth is plotted in (i) and (j). The estuarine exchange flow is evident in both observed and modeled v-velocity fields (a, c, d, g). Currents are rotated to be along the principle axis of the observed hourly current data, which is dominated by tides.*

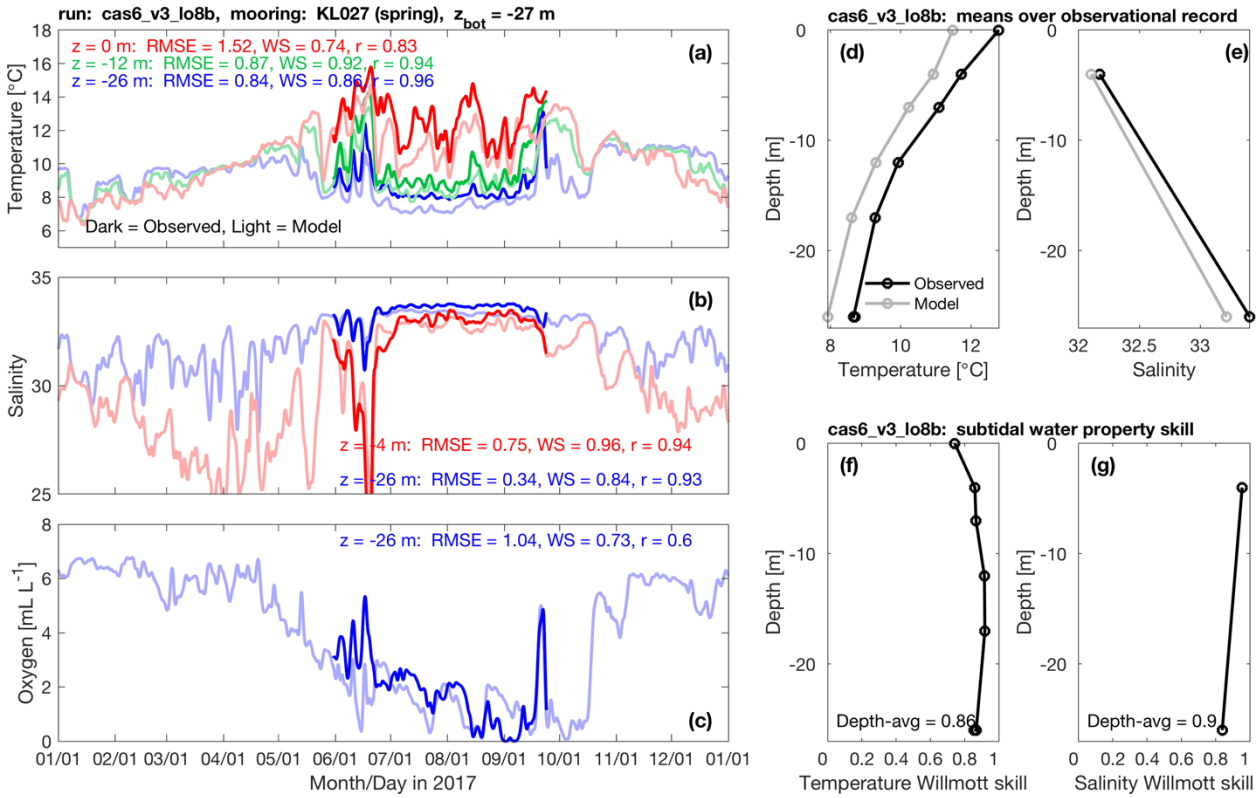

Figure S9. *Mooring comparison on the WA coast from an Olympic Coast National Marine Sanctuary station occupied during the summer of 2017, in 27 m water depth (mooring station "M" in Fig. S1b). Observed fields at 1 or more depths are shown in dark lines in (a-c), with corresponding model lines plotted as transparent. All are tidally filtered. Time averages over the observational period for temperature and salinity are plotted vs. depth in (d) and (e). Corresponding Willmott skills vs. depth are plotted in (f) and (g). Low salinity events, like that in mid-June, correspond to storms with southerly wind pushing the Columbia River plume to the north.*

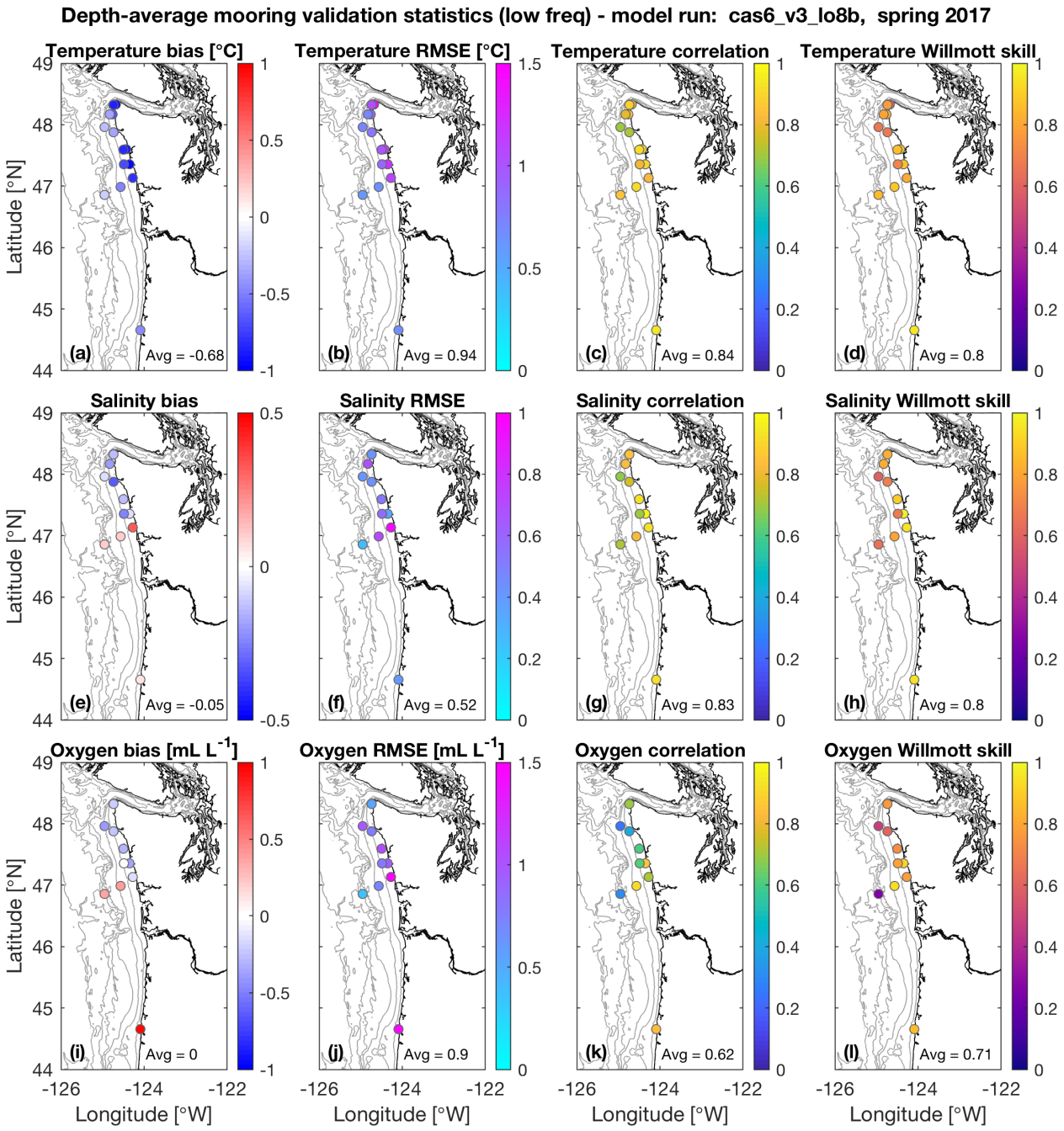

Figure S10*. Depth-averaged validation statistics for 14 moorings on the shelf (colored circles) and an average from all moorings (text values). Observations occurred over some part of the middle of 2017, as in Fig. S9. Plotted are mean bias, RMSE, correlation coefficient (none were negative, hence the 0-1 color rage), and Willmott skill. Variables compared are salinity, temperature, and dissolved oxygen, as labeled.*

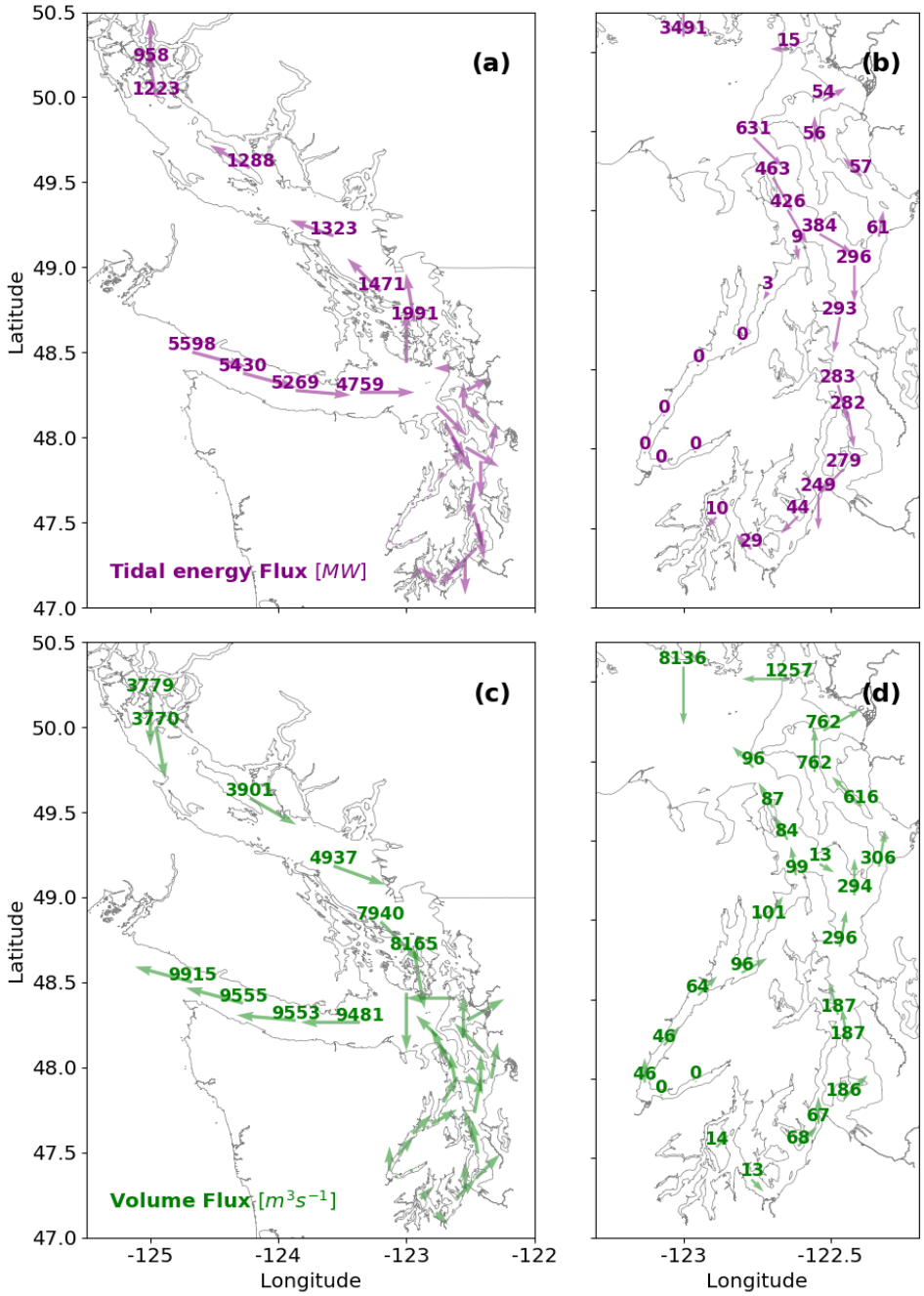

Figure S11*. Tidal energy flux (a, b) and net volume flux (c, d) through all TEF sections, averaged over 2017. Values are omitted at Tacoma Narrows sections tn1 and tn3 for clarity. The direction of the flux is indicated by arrows, and the associated value is shown as a number near the base of the arrow.*

353

354 ***REFERENCES [also included in the main text]***

355

356 Babson, A. L., Kawase, M., & MacCready, P. (2006). Seasonal and Interannual
357 Variability in the Circulation of Puget Sound, Washington: A Box Model Study.
358 *Atmosphere-Ocean, 44*, 29-45. doi:10.3137/ao.440103

359 Brasseale, E., Grason, E. W., McDonald, P. S., Adams, J., & MacCready, P. (2019).
360 Larval Transport Modeling Support for Identifying Population Sources of
361 European Green Crab in the Salish Sea. *Estuaries and Coasts*.
362 doi:10.1007/s12237-019-00586-2

363 Codiga, D. L. (2011). *Unified Tidal Analysis and Prediction Using the UTide Matlab*
364 *Functions*. Retrieved from
365 ftp://www.po.gso.uri.edu/pub/downloads/codiga/pubs/2011Codiga-UTide-
366 Report.pdf

367 Davis, K. A., Banas, N. S., Giddings, S. N., Siedlecki, S. A., MacCready, P., Lessard, E.
368 J., et al. (2014). Estuary-enhanced upwelling of marine nutrients fuels coastal
369 productivity in the U.S. Pacific Northwest. *Journal of Geophysical Research:*
370 *Oceans, 119*(12), 8778-8799. doi:10.1002/2014jc010248

371 Egbert, G. D., & Erofeeva, S. Y. (2002). Efficient inverse modeling of barotropic ocean
372 tides. *Journal of Atmospheric and Oceanic Technology, 19*, 183-204.
373 doi:10.1175/1520-0426(2002)019<0183:EIMOBO>2.0.CO;2

374 Emery, W. J., & Thomson, R. E. (1998). *Data Analysis Methods in Physical*
375 *Oceanography*. Kidlington, Oxford: Elsevier Science.

376 Feely, R. A., Alin, S. R., Carter, B., Bednaršek, N., Hales, B., Chan, F., et al. (2016).
377 Chemical and biological impacts of ocean acidification along the west coast of
378 North America. *Estuarine, Coastal and Shelf Science, 183*, 260-270.
379 doi:10.1016/j.ecss.2016.08.043

380 Finlayson, D. P. (2005). *Combined bathymetry and topography of the Puget Lowland,*
381 *Washington State*. Retrieved from
382 https://www.ocean.washington.edu/data/pugetsound/psdem2005.html

383 Foreman, M. G. G., Walters, R. A., Henry, R. F., Keller, C. P., & Dolling, A. G. (1995).
384 A tidal model for eastern Juan de Fuca Strait and the southern Strait of Georgia. *J.*
385 *Geophys. Res., 100*, 721-740. doi:10.1029/94JC02721
386 Fredrickson, E. K., Wilcock, W. S. D., Schmidt, D. A., MacCready, P., Roland, E.,
387 Kurapov, A. L., et al. (2019). Optimizing Sensor Configurations for the Detection
388 of Slow-Slip Earthquakes in Seafloor Pressure Records, Using the Cascadia
389 Subduction Zone as a Case Study. *Journal of Geophysical Research: Solid Earth,*
390 *124*, 13504-13531. doi:10.1029/2019JB018053
391 Giddings, S. N., & MacCready, P. (2017). Reverse Estuarine Circulation Due to Local
392 and Remote Wind Forcing, Enhanced by the Presence of Along-Coast Estuaries.
393 *Journal of Geophysical Research: Oceans, 122*, 10184-10205.
394 doi:10.1002/2016JC012479
395 Giddings, S. N., MacCready, P., Hickey, B. M., Banas, N. S., Davis, K. A., Siedlecki, S.
396 A., et al. (2014). Hindcasts of potential harmful algal bloom transport pathways
397 on the Pacific Northwest coast. *Journal of Geophysical Research: Oceans, 119*,
398 2439-2461. doi:10.1002/2013JC009622
399 Haidvogel, D. B., Arango, H. G., Hedstrom, K., Beckmann, A., Malanotte-Rizzoli, P., &
400 Shchepetkin, A. F. (2000). Model evaluation experiments in the North Atlantic
401 Basin: simulations in nonlinear terrain-following coordinates. *Dynamics of*
402 *Atmospheres and Oceans, 32*, 239-281. doi:10.1016/S0377-0265(00)00049-X
403 Khangaonkar, T., Long, W., & Xu, W. (2017). Assessment of circulation and inter-basin
404 transport in the Salish Sea including Johnstone Strait and Discovery Islands
405 pathways. *Ocean Modelling, 109*, 11-32. doi:10.1016/j.ocemod.2016.11.004
406 Lavelle, J. W., Mofjeld, H. O., Lempriere-Doggett, E., Cannon, G. A., Pashinski, D. J.,
407 Cokelet, E. D., et al. (1988). *A multiply-connected channel model of tides and*
408 *tidal currents in Puget Sound, Washington and a comparison with updated*
409 *observations*. Retrieved from
410 https://www.pmel.noaa.gov/pubs/PDF/lave967/lave967.pdf
411 Liu, Y., MacCready, P., Hickey, B. M., Dever, E. P., Kosro, P. M., & Banas, N. S.
412 (2009). Evaluation of a coastal ocean circulation model for the Columbia River

plume in summer 2004. *Journal of Geophysical Research, 114*. doi:10.1029/2008jc004929

Mass, C. F., Albright, M., Ovens, D., Steed, R., MacIver, M., Grimit, E., et al. (2003). Regional environmental prediction over the Pacific Northwest. *Bulletin of the American Meteorological Society, 84*, 1353-1366+1328. doi:10.1175/BAMS-84-10-1353

Metzger, E. J., Smedstad, O. M., Thoppil, P., Hurlburt, H., Cummings, J., Walcraft, A., et al. (2014). US Navy Operational Global Ocean and Arctic Ice Prediction Systems. *Oceanography, 27*(3), 32-43. doi:10.5670/oceanog.2014.66

Mohamedali, T., Roberts, M., Sackmann, B., & Kolosseus, A. (2011). *Puget Sound Dissolved Oxygen Model Nutrient Load Summary for 1999-2008* (8778336341). Retrieved from

Shchepetkin, A. F., & McWilliams, J. C. (2005). The regional oceanic modeling system (ROMS): a split-explicit, free-surface, topography-following-coordinate oceanic model. *Ocean Modelling, 9*, 347-404. doi:10.1016/j.ocemod.2004.08.002

Siedlecki, S. A., Banas, N. S., Davis, K. A., Giddings, S. N., Hickey, B. M., MacCready, P., et al. (2015). Seasonal and interannual oxygen variability on the Washington and Oregon continental shelves. *Journal of Geophysical Research: Oceans, 120*(2), 608-633. doi:10.1002/2014jc010254

Sutherland, D. A., MacCready, P., Banas, N. S., & Smedstad, L. F. (2011). A Model Study of the Salish Sea Estuarine Circulation. *Journal of Physical Oceanography, 41*(6), 1125-1143. doi:10.1175/2011jpo4540.1

Sutherland, G., Garrett, C., & Foreman, M. (2005). Tidal Resonance in Juan de Fuca Strait and the Strait of Georgia. *Journal of Physical Oceanography, 35*(7), 1279-1286. doi:10.1175/jpo2738.1

Thomson, R. E., & Huggett, W. S. (1980). M2 Baroclinic Tides in Johnstone Strait, British Columbia. *Journal of Physical Oceanography, 10*, 1509-1539. doi:10.1175/1520-0485(1980)010<1509:MBTIJS>2.0.CO;2

Tozer, B., Sandwell, D. T., Smith, W. H. F., Olson, C., Beale, J. R., & Wessel, P. (2019). Global Bathymetry and Topography at 15 Arc Sec: SRTM15+. *Earth and Space Science, 6*(10), 1847-1864. doi:10.1029/2019ea000658

444